Glacial cycles simulation of the Antarctic Ice Sheet with PISM - Part 1: Boundary conditions and climatic forcing

Torsten Albrecht [1], Ricarda Winkelmann [1,2], and Anders Levermann [1,2,3]

[1]Potsdam Institute for Climate Impact Research (PIK), Member of the Leibniz Association, Potsdam, Germany
[2]Institute of Physics and Astronomy, University of Potsdam, Potsdam, Germany
[3]Lamont-Doherty Earth Observatory, Columbia University, New York, USA

Correspondence to: T. Albrecht (albrecht@pik-potsdam.de)

Abstract. Simulations of the glacial-interglacial history of the Antarctic Ice Sheet provide insights into dynamic threshold behavior and estimates of the ice sheet's contributions to global sea-level changes, for both the past, present and future. However, boundary conditions are weakly constrained, in particular, at the interface of the ice-sheet and the bedrock. Also climatic forcing covering the last

5   glacial cycles is uncertain as it is based on sparse proxy data.

We use the Parallel Ice Sheet Model (PISM) to investigate the dynamic effects of different choices of input data, e.g. for modern basal heat flux or reconstructions of past changes of sea-level and surface temperature. As computational resources are limited, glacial-cycle simulations are performed using a comparably coarse model grid of 16 km and various parameterizations, e.g. for basal sliding,

10   iceberg calving or for past variations of precipitation and ocean temperatures. In this study we evaluate the model's transient sensitivity to corresponding parameter choices and to different boundary conditions over the last two glacial cycles. It hence serves as a 'cookbook' for the growing community of PISM users. We identify relevant model parameters and motivate plausible parameter ranges for a Large Ensemble analysis, which is described in a companion paper.

15 ## 1 Introduction

==Process-based models provide the tools to reconstruct the ice sheet's history and to improve our understanding of involved processes and thresholds and to better anticipate possible future pathways (Pattyn, 2018).== However, ice sheet simulations involve various sorts of uncertainties. The stress balance and thickness evolution of the ice sheet is approximated and discretized, which implies different

20   sorts of model-internal errors that should vanish for finer model grids (Gladstone et al., 2012; Pattyn

et al., 2013). Parameterizations of physical processes at the interfaces of the ice with bedrock, ocean or atmosphere, such as basal friction, isostatic rebound, sub-shelf melting or accumulation of snow at the ice surface, involve uncertain model parameters (e.g., Gladstone et al., 2017). Certain feedback mechanisms associated with self-sustained calving may be relevant for warmer than present

25   climates, but not for the last glacial cycles (Edwards et al., 2019). Coupled climate-ice sheet systems models are computationally too expensive in order to run many long simulations. The climatic history can be instead approximated with the modern climate mean scaled by temperature anomaly time series based on single ice cores reconstructions, which involve significant methodological uncertainties though (Cuffey et al., 2016; Fudge et al., 2016). Uncertainties are also large for available

30   indirect observations of boundary conditions, e.g. for the bed topography (Sun et al., 2014; Gasson et al., 2015) or till properties underneath the ice sheet and ice shelves (Brondex et al., 2017; Falcini et al., 2018).

In order to gain confidence in model reconstructions and hence in future model projections, uncertain model parameters need to be constrained and calibrated (Briggs et al., 2014) using a Large Ensemble

35   analysis (Pollard et al., 2016), as demonstrated in a systematic way in a companion paper (Albrecht et al., 2019). This study motivates choices of boundary conditions and climatic parameterizations for application in large-scale paleo ice-sheet simulations and provides an assessment of the associated sensitivity of the model's response. Therefore, we run simulations of the entire Antarctic Ice Sheet with the Parallel Ice Sheet Model (Winkelmann et al., 2011; The PISM authors, 2017) and describe

40   a spin-up procedure for uncertain state variables, such as the three-dimensional enthalpy field or the till friction angle at the base. The hybrid of two shallow approximations of the stress balance and the comparably coarse resolution of 16 km enable computationally efficient simulation of ice sheet dynamics over the last two glacial cycles, each lasting for about 100,000 years (or 100 kyr, Lisiecki, 2010).

45   Section 1.1 describes the ice sheet model and Sect. 2 assesses the sensitivity for parameter variations of the ice sheet model dynamically coupled to an Earth model. Sections 3 and 4 describe the used boundary conditions and climatic forcing, respectively, and discuss how they contribute to the sea-level relevant ice volume history. The analysis is complemented by perturbation experiments in Sect. 5. In the conclusions we identify a subset of the most relevant parameters as used in the Large

50   Ensemble analysis in a companion paper (Albrecht et al., 2019).

1.1 PISM

The Parallel Ice Sheet Model (PISM[1]) is an open-source three-dimensional ice-sheet model (Winkelmann et al., 2011; The PISM authors, 2017) that is used in a growing community for sea-level projections (e.g. Winkelmann et al., 2015; Golledge et al., 2015, 2019) and regional studies (e.g. Mengel

55   and Levermann, 2014; Feldmann and Levermann, 2015; Mengel et al., 2016). It uses a hybrid combi-

---

[1]http://www.pism-docs.org, see also Section 'code and data availability'

nation of two stress balance approximations for the deformation of the ice, the Shallow Ice-Shallow Shelf Approximation (SIA-SSA), that guarantees a smooth transition from vertical-shear-dominated flow in the interior via sliding-dominated ice-stream flow to fast plug flow in the floating ice shelves (Bueler and Brown, 2009), while neglecting higher-order modes of the flow. Driving stress at the

60   grounding line is discretized using one-sided differences (Feldmann et al., 2014). Using a sub-grid interpolation scheme (Gladstone et al., 2010) the grounding line location simply results from flotation condition, without additional flux conditions imposed. Basal friction and basal melt is interpolated accordingly. Thus, grounding-line migration is reasonable well represented in PISM (compared to full Stokes), even for coarse resolution (Pattyn et al., 2013; Feldmann et al., 2014). Ice deforms

65   according to the Glen-Paterson-Budd-Lliboutry-Duval flow law connecting strain rates $\dot{\epsilon}$ and deviatoric stresses τ for enhancement factor E, flow law exponent n and ice softness A, that depends on both liquid water fraction ω and temperature T (Aschwanden et al., 2012),

$$\dot{\epsilon}_{ij} = \mathrm{E} \cdot A(T,\omega)\, \tau^{n-1} \tau_{i,j}. \tag{1}$$

PISM simulates the three-dimensional polythermal enthalpy conservation for given surface temperature and basal heat flux to account for melting and refreezing processes in temperate ice (Aschwanden and Blatter, 2009; Aschwanden et al., 2012). The energy conservation scheme also accounts for the production of sub-glacial (and transportable) water (Bueler and van Pelt, 2015), which affects basal friction via the concept of a saturated and pressurized sub-glacial till. With a modeled distribution of yield stress this allows for grow-and-surge instability (Feldmann and Levermann, 2017;

75   Bakker et al., 2017). Here we use the non-conserving hydrology model, where the till water content in each grid cell is balanced by basal melting and a constant drainage rate.

Iceberg formation at ice shelves is parameterized based on spreading-rates (Levermann et al., 2012). Ice shelf melting is calculated using the Potsdam Ice-shelf Cavity mOdel (PICO), that considers ocean properties in front of the ice shelves and simulates vertical overturning circulation in

80   the ice-shelf cavity (Reese et al., 2018).

PISM uses a generalized version of the Lingle-Clark bedrock deformation model (Bueler et al., 2007), assuming an elastic lithosphere, a resistant asthenosphere and a spatially-varying viscous half-space below the elastic plate (Whitehouse, 2018). The computationally-efficient bed deformation model has been improved to account for changes in the load of the ocean layer around the grounded

85   ice sheet, due to changes in sea-level and ocean depth.

A continental-scale representation of modern bed topography is obtained from the Bedmap2 dataset (Fretwell et al., 2013) and modern uplift rates as initial condition from Whitehouse et al. (2012). We simulate the entire Antarctic continent with 16 km grid resolution compatible with the definition of the initMIP model intercomparison project (Nowicki et al., 2016).

90   PISM paleo simulations are initiated with a spin-up procedure ~~for prescribed~~ ice sheet geometry, in which the three-dimensional enthalpy field can adjust to mean modern climate boundary conditions over a 200 kyr period. Full glacial dynamics are then simulated over the last two glacial cycles with

a forcing starting in the penultimate interglacial (210 kyr BP, before present) and run until the year

2000 AD (-50 yr BP). The sensitivity of the modeled ice volume above flotation to different choice of

95 parameters and boundary conditions is evaluated as the difference to a baseline simulation (Movie: Albrecht, 2019) that is consistent with the model configuration of the best fit simulation presented in a companion paper (Albrecht et al., 2019).

1.2 Volume above flotation

In order to compare ice volume histories we calculate the associated contribution to global mean

100 sea-level in units of 'm SLE'. Be aware that many studies just convert grounded ice volume (in units of 'million km^3') into more handy units of sea-level equivalents (using conversion factors between 2.4 and 2.8), without subtracting the portion of the ice volume that is grounded below flotation. If this fraction of ice resting on deep submarine beds is lost, its mass converts to water required to fill the same basin (almost) without changing sea-level. Analogous to the 'volume above flotation' by

105 the SeaRISE model intercomparison (Bindschadler et al., 2013, Eq. 1), we define here

$$
\begin{aligned}
V_{\mathrm{SLE}} &= \frac{\rho_i}{\rho_o} \operatorname{sum}(H\, c_a)/A_o \quad \text{if} \quad H > \max(10, h_{\mathrm{f}}) \\
&- \operatorname{sum}[(z_{\mathrm{sl}} - b)\, c_a]/A_o \quad \text{if} \quad H > \max(10, h_{\mathrm{f}}) \quad \text{and} \quad h_{\mathrm{f}} > 0, \\
h_{\mathrm{f}} &= \frac{\rho_o}{\rho_i}\,(z_{\mathrm{sl}} - b),
\end{aligned}
\tag{2}
$$

where H is the full ice thickness above a threshold of 10 m, h_{f} the flotation height, c_a is the area distribution among grid cells (corrected for stereographic projection), $z_{\mathrm{sl}} - b$ is the water depth for current sea level z_{sl} and bedrock topography b and $\rho_o = 1028\,\mathrm{kg\,m^{-3}}$ and $\rho_i = 910\,\mathrm{kg\,m^{-3}}$ are the

110 densities of sea water and ice, respectively (see also Table 1). For consistency reasons with the used PISM version, we use ocean water density here. In fact, a density of 1000 kg m^{-3} should be used instead as ice melts to fresh water. Hence, the anomaly $\Delta V_{\mathrm{SLE}}(t)$ is calculated from the total Antarctic ice above flotation for current sea level forcing z_{sl} and evolving bedrock topography b, divided by global ocean area $A_o = 3.61 \times 10^{14}\,\mathrm{m^2}$, relative to the value for the modern observed ice

115 sheet (Bedmap2; Fretwell et al., 2013).

2 Ice sheet and Earth model parameters

PISM solves a coupled system of model equations for the conservation of energy, momentum and mass. Model equations are discretized using a regular rectangular grid of 16 km resolution. Equations of stress balance are simplified using a hybrid of the shallow approximations SIA and SSA, which

120 allows PISM to run glacial cycles simulations simulations. In order to close the equation system, ice sheet models commonly use a flow law (Eq. (1)), which relates ice flow to stresses. It is a result of empiric measurements and statistics for rather idealized conditions, such that the flow law fitting exponent is no fixed physical constant. Enhancement factors compensate for unresolved rheological

effects, e.g. anisotropy. In this section we want to understand effects of ice sheet and Earth model
125   parameter variations on the transient glacial cycle ice sheet response.

2.1 Ice rheological flow law exponent

Generations of ice sheet modelers used variants of Glen's flow law (Eq. (1)) as constitutive relation-
ship between stress and internal flow with the rheological exponent $n = 3$. According to an analysis
of data in Greenland by Bons et al. (2018) the ice rheological exponent for the SIA stress balance
130   should be rather $n = 4$. For same strain rates at reference pressure of $50\,\mathrm{kPa}$, we would need to adjust
the ice softness factor A accordingly. In the model, the same effect is achieved when adjusting the
SIA enhancement factor ESIA$= 2.0$ divided by $50{,}000\,\mathrm{Pa}$ yields $4.0 \cdot 10^{-5}$ instead.

We have tested the effect of the flow law exponent $n = 4$ (and $n = 2$ to cover the range according
to Goldsby and Kohlstedt (2001)) in comparison to the reference simulation and find only small
135   differences in the ice volume time series with on average less than $0.9\,\mathrm{m}$ SLE difference (Fig.1).
However, the flow law exponent for the SSA has much stronger effects on ice volume with 2–
$7\,\mathrm{m}$ SLE less Antarctic ice volume for $n = 4$ and significantly earlier deglaciation, while for $n = 2$
deglaciation is damped effectively.
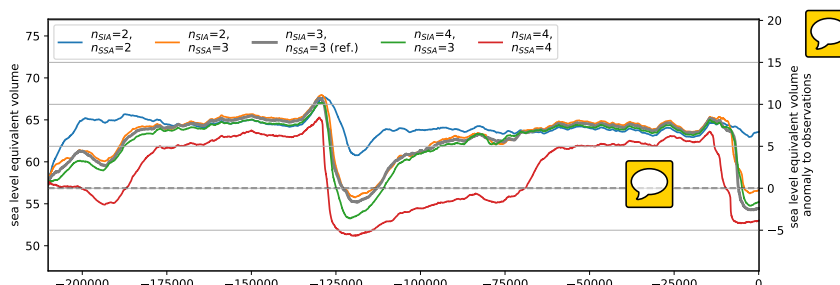
Figure 1: Simulation over two glacial cycles with different flow law exponents in the SIA stress
balance, varying from 2–4 (orange, grey, green). Enhancement factor has been adjusted such that
stress balances compares at $50\,\mathrm{kPa}$. The impact of the choice of the exponent for the SIA stress
balance on the simulated ice volume above flotation is rather small. In contrast, variation of the SSA
flow law exponent strongly affects ice sheet growth and deglaciation (red and blue).

2.2 Model grid resolution

140   Resolution is a key parameter which determines the misfit between the model results based on dis-
cretized model equations and analytical solutions. Analytical solutions for the coupled system of ice
sheet model equations can only be found for simplified flow line configurations. For the more real-
istic case we can get some impression of resolution requirements if we run regression tests to show

that grid refinement leads to a convergence of the model solution. Resolution of the boundary data

145 in turn can control key parameters of ice stream flow, such as basal roughness (Falcini et al., 2018).
We also test for the vertical resolution of the three-dimensional enthalpy field here, which is highest
at the ice sheet's base and lowest at the top of the computational domain using a quadratic spacing.
The enthalpy formulation allows the transition from cold to temperate ice (Aschwanden et al., 2012),
which can form temperate ice layers of up to a few hundred meters.

150   We find that for our reference parameters and 16 km resolution a similar ice volume history can
be reconstructed as for 8 km resolution, while computation costs are about a factor of 10 higher (see
Fig. 2). For much coarser grids of the order of 30 km or more (Briggs et al. (2014) used 40 km) we
find that relevant ice streams dynamics cannot be resolved any more in an adequate way (Aschwan-
den et al., 2016). In Fig. 2 we find how resolution can effect glacial-interglacial ice volume history

155 with more than 5 m SLE difference, resulting in very different modern ice sheet configurations (see
blue line in Fig. 2). In fact, also for coarse resolution we may find solutions that are closer to the
reference simulation, e.g. by choosing different enhancement factors.

    For the vertical grid we define highest grid spacing at the base with a resolution of around 20 m
in the reference simulation. Coarser vertical resolution (doubled spacing) does not change the sim-

160 ulation result much (green line in Fig. 2). For finer resolution shear heating and the formation of
temperate ice is expected to be better resolved and the simulation results should converge. However,
the simulated ice volume seems to increase by 3–5m SLE for doubling vertical resolution (see red
line in Fig. 2), as less temperate ice is formed in the lowest layers of the ice sheet. Benchmark ex-
periments with respect to an analytical enthalpy solution (Kleiner et al., 2015) suggests adequate

165 convergence for vertical resolution finer than 1 m at the base (see violet line in Fig. 2).
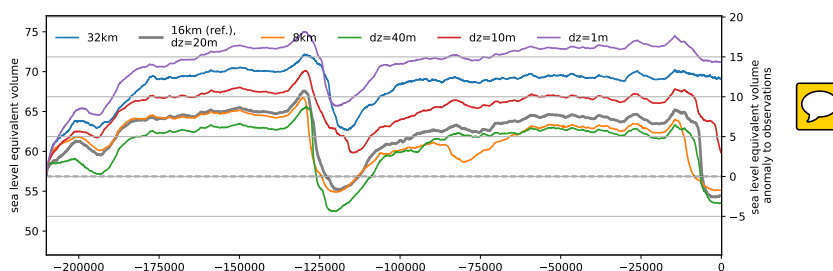
Figure 2: Simulated volume above flotation over two last glacial cycles with reference resolution of
16 km (grey), fine grid resolution of 8 km (blue) and relatively coarse resolution of 32 km (orange)
resulting in different Antarctic Ice Sheet histories. Refined vertical resolution of 10 m (red) and 1 m
(violet) at the base is compared to the reference simulation with 20 m and with coarse resolution of
40 m (green).

2.3 Ice flow enhancement factors

Enhancement factors account for unresolved effects of grain size, fabric and impurities and have often been used as tuning parameter in ice sheet modeling entering the constitutive flow law (Eq. (1)) that balances strain rates and stresses within the ice sheet. Value 1 means 'no enhancement', but

170 generally enhancement factors for the SSA tend to be smaller than 1 and larger than 1 for the SIA. Anisotropic ice-flow modeling suggests E_{SSA} values between 0.5 and 0.7 for ice shelves and between 0.6 and 1 for ice streams, while for SIA enhancement should lie between 5 and 6 (Ma et al., 2010). Previous model ensembles that consider isotropic ice flow use values down to $E_{SSA} = 0.3$ (for $E_{SIA} = 1$) in (Pollard and DeConto, 2012a, PSU model) or up to $E_{SIA} = 9$ (for $E_{SSA} = 0.8$) in

175 (Maris et al., 2014, ANICE model), both for 20 km resolution. PISM seems to favor enhancement factors closer to 1 (e.g. $E_{SSA} = 0.5$–0.6 and $E_{SIA} = 1.2$–1.5 in (Golledge et al., 2015) for 10–20 km resolution).

Figure 3 shows the effects of ice flow enhancement factors on simulated Antarctic Ice Sheet history. SIA enhancemnet generally produces thicker grounded ice. Compared to the reference sim-

180 ulations with $E_{SIA} = 2$ the model simulates for $E_{SIA} = 1$ more than 5 m SLE thicker and for $E_{SIA} = 5$ about 6 m SLE thinner ice sheets, both at glacial and interglacial states (blue and orange). The effect of E_{SSA} variation is most predominant for ice sheet growth and for deglaciation, when ice flow across the grounding line influences its migration and stabilization (Schoof, 2007b). For $E_{SSA} = 1$ (green) we find earlier retreat and hence 1–2 m SLE thinner modern ice sheets than for $E_{SSA} = 0.6$

185 (grey reference). For lower values of $E_{SSA} = 0.3$ (red), in contrast, deglaciation is limited and modern ice volumes are more than 5 m SLE thicker than observations. This is because larger values of the SSA enhancement factor produce faster ice streams and thinner ice shelves. We hence find the SIA enhancement factor, 'ESIA', a suitable ice-internal parameter candidate for the ensemble analysis in Albrecht et al. (2019).
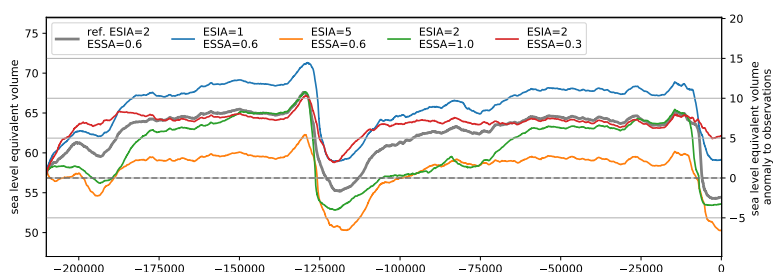
Figure 3: Ice volume above flotation for simulations over two last glacial cycles with varied enhancement factors for SIA and SSA stress balance. Larger E_{SIA} lead to thicker grounded ice sheets, while larger E_{SSA} cause faster deglaciation and slightly thinner modern ice sheets.

2.4 Iceberg calving

Currently, calving constitutes almost half of the mass loss from the Antarctic Ice Sheet (Depoorter et al., 2013). PISM provides different schemes for iceberg calving. For floating ice shelves we use the strain-rate based *eigencalving* parameterization, which accounts for the average tabular iceberg calving flux depending on ice shelf flow and confinement geometry (Levermann et al., 2012; Albrecht and Levermann, 2014). The minor eigenvalue of the horizontal strain rate basically determines where calving can occur, e.g. in the expansive flow regions beyond a critical arch between outer pinning points of ice rises or mountain ridges (Doake et al., 1998; Fürst et al., 2016). The average eigen-calving rate is the product of minor and major eigenvalue of the horizontal strain rate scaled with a constant. In our simulations we use a parameter value of K$= 1 \times 10^{17}$ m s. For a much larger value of 1×10^{18} m s calving front tends to retreat, limited by the location of the compressive arch. Smaller ice shelves exert less buttressing on the ice flow and we find s slower ice sheet growth for glacial climate conditions (see Fig. 4). For a smaller value of 1×10^{16} m s estimated calving rates tend to be smaller than terminal ice shelf flow and thus calving front expands. In our simulations we define a m~~yy~~ ~~mal~~ extent for ice shelves where the present ocean floor drops below 2 km depth, assuming that ice shelves can only exist on the shallow continental shelf. Additionally we avoid very thin ice shelves below 75 m, as enthalpy field evolution and hence the ice flow can not adequately be represented for only a few vertical grid layers. Hence, ice at the calving front thinner than 75 m is removed. Both calving conditions are applied mainly for numerical reasons (adaptive time stepping) to avoid thin ice tongues, but they have negligible influence on the simulated ice volume history. For higher lower bounds of terminal ice thickness of 150 m or even ~~m~~ 225 m, as often used in other model studies, we find slower ice sheet growth but negligible effect on deglaciation and interglacial ice volume (see Fig. 4. As eigencalving supports ice shelves within confinements we find that the effects of ice shelf extent beyond its compressive arch is of relatively low relevance for the glacial-interglacial ice sheet history. This is in contrast to previous model ensembles, who diagnosed high sensitivity of simulation results to varied calving parameters using different calving parameterizations (Briggs et al., 2013; Pollard et al., 2016)
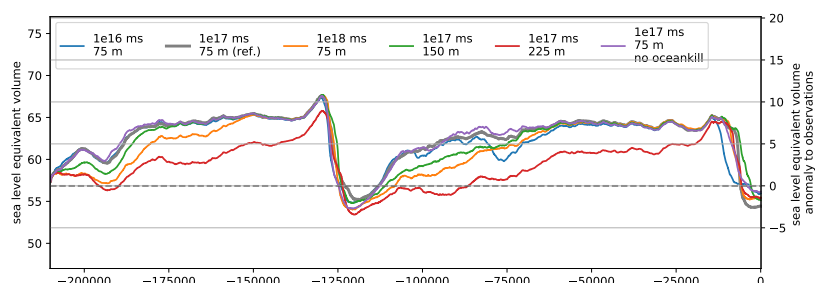
Figure 4: Ice volume histories over two glacial cycles for different parameter values of eigencalving constant (blue and orange) and calving thickness (green and red) compared to the reference simulation (grey). Defining a maximum extent of the ice along the edge of the continental shelf has only negligible effect on the sea-level relevant ice volume (violet).

2.5 Mantle viscosity and flexural rigidity

We have shown that sea-level changes drive grounding line migration (in particular in deglaciation processes) through the flotation criterion (see Sect. 4.1). In fact sea-level changes at the grounding

220   line are not only caused by global mean sea-surface height change but also by local changes in the sea floor and bed topography. PISM incorporates an Earth model that reflects the deformation of an elastic plate overlying a viscous half-space. A key advantage this approach ~~has~~ over traditional Elastic Lithosphere Relaxing Asthenosphere (ELRA) models is that the response time of the sea floor is not considered a constant, but depends on the wavelength of the load perturbation for a

225   given Asthenosphere viscosity (Bueler et al., 2007). Calculations are carried out using the computationally efficient Fast Fourier Transform to solve the biharmonic differential equation for vertical displacement in response to (ice) load changes σ_{zz} (Bueler et al., 2007, Eq. 1). The Earth model can be initilized with a present-day uplift map (Whitehouse et al., 2012). The formulation closely approximates the approach used within many GIA models (Whitehouse, 2018), which are defined to

230   account for the response of the solid Earth and the global gravity field to changes in the ice and water distribution on the ~~entire~~ Earth's surface (Whitehouse et al., 2019). With ~~our~~ approach we can also account for vertical displacement in response to spatially varying water-load changes. However, our Earth model is not yet able to account for self-consistent gravitational effects associated with local sea-level variations or the rotational state of the Earth (Gomez et al., 2013; Pollard et al., 2017).

235

We investigate two relevant parameters of the Earth model with regard to the viscous and the elastic part.. *Mantle viscosity* affects model behaviour because it defines the rate and pattern of the deformation of the ice-sheet's bed and the sea floor. Antarctic Ice Sheet models typically use mantle

viscosity of 1×10^{21} Pa s. Our reference simulation uses a mantle viscosity of 5×10^{20} Pa s to account
240 for the weaker mantle beneath the WAIS (Hay et al., 2017; Barletta et al., 2018).

In our glacial-cycle simulations an even lower mantle viscosity of 1×10^{20} Pa s results in delayed
deglaciation and thicker present-day ice sheets than for the reference value of 5×10^{20} Pa s (cf. grey
and blue in Fig. 5a). As the bed at the grounding line responds faster to unloading for lower vis-
cosities, grounding line retreat is hampered accordingly. In contrast, more viscous mantles of 25–
245 100×10^{20} Pa s result in slower ice sheet growth but in faster deglaciation and hence lower present-
day ice volumes above flotation (orange and green in Fig. 5a). ==Within a plausible range== the effect of
mantle viscosity on grounding line retreat and re-advance since last deglaciation has been discussed
in Kingslake et al. (2018).

The bed deformation model in PISM up to v1.0 considered all changes in ice thickness H as
250 loads[2], including changes in ice shelf thickness, although this does not make physical sense. Here
we ==presented== simulations that consider changes in load of the grounded ice sheet and of the ocean
layer within the computational domain with load per unit area defined as

$$\sigma_{zz} = \rho_i \left[\max\left(H - h_f, 0.0\right) + h_f\right], \tag{3}$$

with h_f the flotation height as defined in Eq. (2). Our simulations that considers changes in ocean
255 loads yields up to 3 m SLE higher ice volumes above flotation at glacial maximum, while inter-
glacial ice volumes are comparable (*cf.* grey and red lines in Fig. 5a and violet line in Fig. 5b, which
excludes both ocean and ice shelf loads as in PISM v1.1). Also, deglaciation is delayed by a few
thousand years.

260 *Flexural rigidity* is associated with the thickness of the elastic lithosphere and has an influence
on the horizontal extent to which bed deformation responds to changes in load. We have deactivated
the elastic part of the Earth model in our reference simulation, as the numerical implementation was
flawed. Instead we have used PISM v1.1, which considers only grounded ice thickness changes as
loads, with additionally fixed elastic part[3], in order to evaluate the ice sheet volume's sensitivity to
265 changes in the flexural rigidity parameter value. As most dynamic changes on glacial cycles occur in
West Antarctica previous studies based on gravity modelling suggest appropriate values lying within
the range of 5×10^{23} N m and 5×10^{24} N m (Chen et al., 2018). The PISM default value marks the
upper end of this range, assuming a thickness of 88 km for the elastic plate lithosphere (Bueler et al.,
2007).
270 For this range extended to 1×10^{25} N m, which is more than an order of magnitude, we find differ-
ences in ice volume above flotation of up ot 4 m SLE, with enhanced temporal variability, see Fig. 5b.
Compared to the reference simulation without the elastic part, we find earlier deglacial retreat but
similar glacial and interglacial volumes.

---

[2]until commit https://github.com/pism/pism/commit/4b5e14037 from April, 2018
[3]https://github.com/pism/pism/issues/424
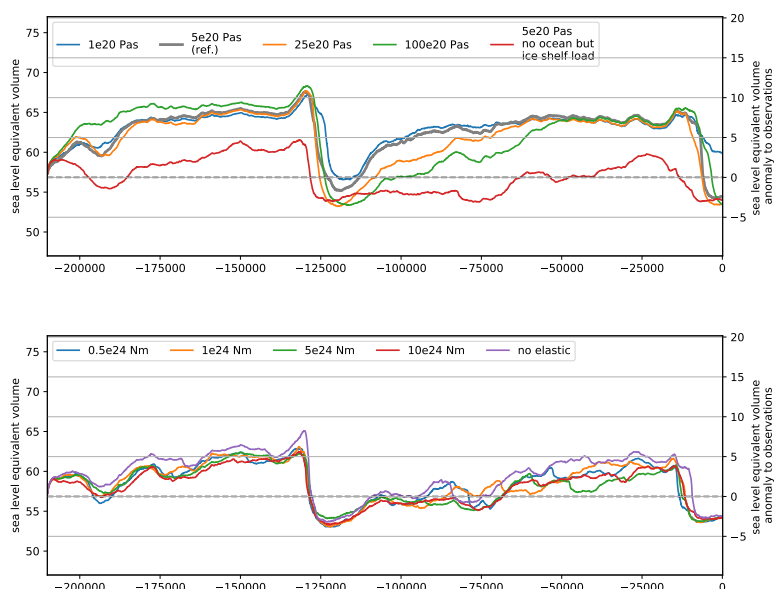
Figure 5: Simulations over two last glacial cycles with varying Earth model parameters for the viscous (a) and the elastic part (b). Mantle ~~viscosity~~ with a range over two orders of magnitude cause slower ice sheet growth but faster decay for increasing viscosity, with up to 5 m SLE difference in ice volumes. Flexural rigidity that ranges over more than one order of magnitude yields smaller difference in simulated ice volumes above flotation, but ~~enhanced~~ variability. Be aware that for the lower panel a different PISM v1.1 has been used with a fixed elastic model. PISM v1.1 accounts for grounded ice loads only and reduces glacial volume by a few meters SLE (violet in lower panel) as compared to the reference (grey in upper panel), while modern ice volumes are similar. If only changes in ice load are considered (including changes in ice shelf thickness as in PISM v1.0, but no changes in the load of the ocean water load) then glacial ice volume is estimated up to 6 m SLE lower (red in upper panel).

3 Boundary conditions and input datasets

3.1 Air temperature

Air temperature is an important surface boundary condition for the enthalpy evolution which is thermodynamically-coupled to the ice flow. The annual and summer mean temperature distribution is required in the Positive-Degree-Day scheme (PDD) to ~~estimates~~ surface melt and runoff rates, assuming a sinusoidal yearly temperature cycle (Huybrechts and de Wolde, 1999, Eqs. C1-3). Hitherto,

280   surface temperatures for Antarctica have been often parameterized based on a multiple regression fit
to reanalysis data, e.g. as a function of latitude lat and surface elevation h. This provides a tempera-
ture field that adjusts to a changing geometry with a prescribed lapse rate and is hence convenient for
paleo time-scale simulations. Using ERA Interim C20 data (Simmons, 2006) multiple regression fit
of summer mean temperatures (January) provides a temperature distribution with a RMSE of 2.2 K

285   over the entire ice sheet, while for annual mean temperatures the RMSE is 4.1 K. Temperatures are
considerably overestimated by up to 11 K over the large Ronne and Ross ice shelves and in large
parts of inner East Antarctica, while temperatures in dynamically relevant regions along the West
Antarctic Divide are underestimated by up to -5 K.

Regarding the comparably shallow ice shelves with less than 100 m surface height, this surface-

290   height dependent parameterization estimates temperature close to those on the sea surface, although
observed climatic conditions on the large ice shelves are much colder than those on the ocean (prob-
ably effects of albedo and catabatic winds). As a correction we assume that the ice shelves' surface
(and all other icy regions below 1000 m altitude for consistency) is as cold as at 1000 m altitude to
achieve a better fit to ERA-Interim data. Furthermore, the climate in the much larger East Antarctic

295   Ice Sheet is more isolated than the climate in West Antarctica which can be accounted for with a
longitudinal dependence lon and symmetry axis through the West Antarctic Divide (110°W), as

$$T_{\text{aml}} \quad = 37.5 - 0.0095 \cdot \max(h, 1000) - 0.644 \cdot lat + 2.145 \cdot \cos\left(lon + 110°\right) \tag{4}$$

$$T_{\text{sml}} \quad = 15.7 - 0.0083 \cdot \max(h, 1000) - 0.196 \cdot lat + 0.225 \cdot \cos\left(lon + 110°\right). \tag{5}$$

Summer temperatures T_{sml} are well represented by Eq. (5) with a RMSE of 2.1 K over the entire

300   ice sheet and a particularly good match in the large ice shelves and East Antarctica. Annual mean
temperatures T_{aml} parameterized by Eq. (4) are overestimated by less than 5 K both in the inner
East Antarctic Ice Sheet and the large ice shelves of Ross and Ronne-Filchner (see Fig. 6), while
temperatures in the West Antarctic Ice Sheet are underestimated by less than 1 K (RMSE 3.1 K).
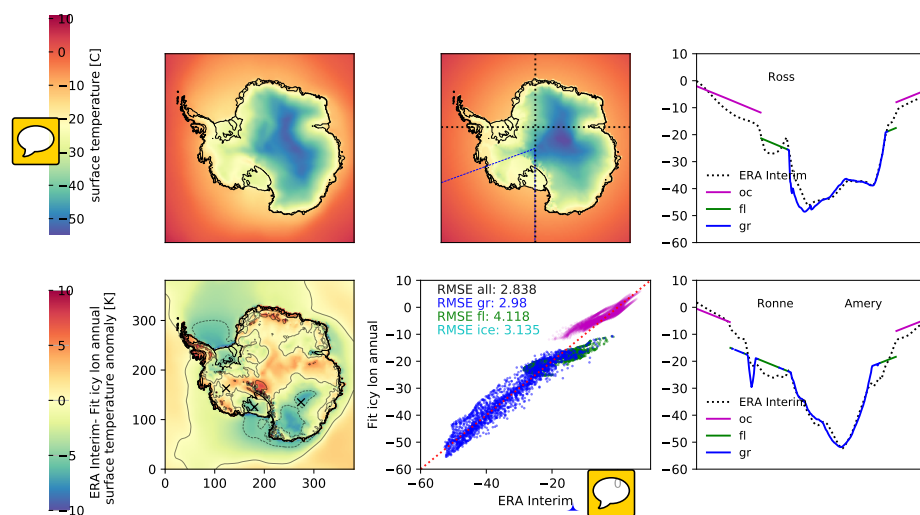
Figure 6: Comparison of ERA Interim annual mean temperatures (a) with parameterization of Eq. (4) with 110°W-longitude indicated as blue-dashed line (b). Inner parts of the West Antarctic Ice Sheet are less than 1 K too cold (d), while temperatures in the shallow ice shelves of Ross and Ronne are overestimated by up to 5 K (cf. panels c and f). Root-mean-square-errors of temperatures in grounded and floating ice sheet regions are 3.0 K and 4.1 K respectively (e).
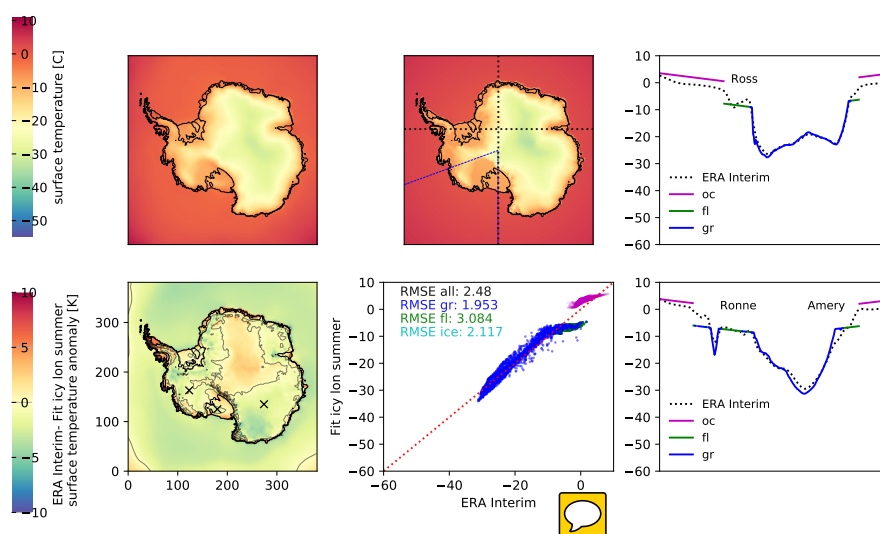
Figure 7: Comparison of ERA Interim summer (January) mean temperatures with parameterization of Eq. (5). Root-mean-square-errors of temperatures in grounded and floating ice sheet regions are 2.0 K and 3.1 K respectively, with temperatures in the large ice shelves close to observations.

The annual mean and summer air temperatures enter the PDD scheme, to calculate melt rates and
305 runoff at the surface. We assume melt rates snow and ice of 3.0 and 8.8 mm for each day and per each degree above freezing point, assuming a daily temperature variability represented by a normally distributed white noise signal with 5 K standard deviation.

In order to evaluate the transient effects of the choice of the modern climate boundary conditions we run two-glacial cycle paleo simulation with climatic forcing that is introduced in following
310 sections of the paper. Here we compare the simulated histories of the ice sheet's 'volume above flotation' with respect to different modern surface temperatures and PDD settings. Lower temperature standard deviation in the PDD scheme of 2 K instead of 5 K has no influence on glacial volume but it can delay deglaciation slightly. Generally, the effect of the PDD scheme for Antarctic paleo simulations seems of minor relevance, see Fig. 8. Even if we omit the PDD scheme and use more
315 realistic annual mean temperature pattern from Racmo2.3p2 (Wessem et al., 2018) or ERA-Interim (Simmons, 2006), simulated ice volumes differ most from the parameterized surface temperature (Sect. 3.1) for interglacial and modern climate forcing with up to 2 m SLE.
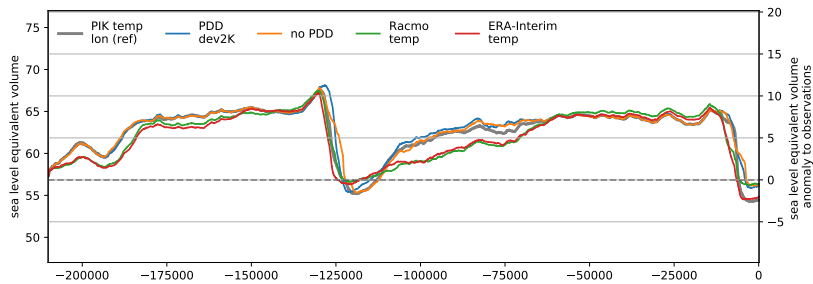
Figure 8: Sensitivity of simulated glacial cycles ice volume to different surface temperatures is low for different PDD standard deviations of 5 K (reference), 2 K and when off. More realistic annual mean surface temperatures from Racmo2.3p2 (Wessem et al., 2018) or ERA-Interim (Simmons, 2006) but without PDD show difference in volume above flotation at the onset of ice sheet growth and in interglacials.

3.2 Precipitation

The distribution of mean precipitation over the Antarctic continent is related to temperatures, but its pattern is strongly determined by the moisture transport over the ice and mountain surface, such that parameterizations as for the temperature (see previous Sect. 3.1) are rather unrealistic. A more realistic near-surface climate, surface mass balance and surface energy balance has been simulated with a resolution of 27 km using a regional atmospheric climate model forced with re-analysis data for the recent past (mean over CMIP5 reference period 1986-2005), such as RACMO2.3p2 (Wessem et al., 2018), which incorporates all relevant physical processes at the ice surface. Similar as for the temperature parameterization we apply a lapse correction for the precipitation field for changing surface elevation Δh, which is defined as

$$\Delta P(\Delta h) = P_0 \exp\left(f_p \Delta T(\Delta h)\right) = P_0 \exp\left(f_p \gamma_T \Delta h\right). \tag{6}$$

with f_p=7%/K a precipitation change factor with temperature and γ_T=7.9 K/km the temperature lapse rate. This correction ensures that topographical changes have an influence on local precipitation through their effect on local surface temperature. However, as re-analysis and regional climate models tend to underestimate present-day precipitation in the interior of the East Antarctic Ice Sheet, simulated ice volume may be biased towards lower than observed values (Van de Berg et al., 2005).

3.3 Basal heat flux

Geothermal heat flux is one of the most poorly known boundary conditions that controls ice flow (Pittard et al., 2016). It can keep basal ice relatively warm, and thus less viscous than colder ice above. In combination with enhanced supply of melt-water at the ice sheet base it supports rapid ice

flow by sliding over the bed and deformation of the subglacial sediments (see previous Sect. 3.4.2).
Various maps with substantially different pattern derived from satellite magnetic and seismological
340 data have been made available for the whole Antarctic continent[4] and were used in ice-sheet model
simulations for longer then a decade now (Shapiro and Ritzwoller, 2004; Fox Maule et al., 2005;
Purucker, 2013; An et al., 2015). Due to their sparse data coverage and significant methodological
uncertainty some modelers decided using a simplified two-valued heat-flux pattern that distinguishes
the geology of the East and West Antarctic plate (Pollard and DeConto, 2012a). In our simulations
345 we use the latest high resolution heat flux map by Martos et al. (2017), which is derived from spectral
analysis of the most advanced continental compilation of airborne magnetic data.

For the different Antarctic basal heat flux data sets we compare PISM simulated quasi-equilibria
after 50 kyr with constant boundary conditions and find only little differences with about 21 m RMSE
between the resulting ice thickness distributions (Fig. 9).
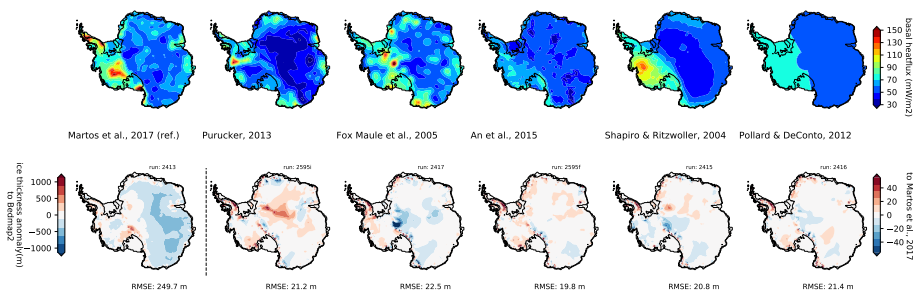
Figure 9: PISM present-day equilibrium results after 50 kyr simulation for different basal heat flux
fields (upper) affecting the near-ground temperatures and hence the ice thickness, here shown as
anomaly to Bedmap2 (first panel in lower row) or relative to the first PISM result. First three columns
show the results for the magnetic reconstructions by Martos et al. (2017), Purucker (2013) and
Fox Maule et al. (2005). Column 4 to 5 shows the seismic reconstructions by An et al. (2015)
and Shapiro and Ritzwoller (2004), and last column for comparison a two-valued field as used in
Pollard and DeConto (2012a), separating East and West Antarctica. The overall effect of the choice
of geothermal heatflux on present-day ice thickness equilibrium is comparably small with up to 50 m
ice thickness anomaly in individual spots in West Antarctica and a RMSE of around 21 m.

350 Here we compare the simulated histories of ice sheet 'volume above flotation' with respect to
the different basal heat flux boundary conditions. The overall effect on ice volume history seems
rather small with a variation of 1.7 m SLE in the present-day result, except for An et al. (2015)
with 6 m SLE above the reference (see Fig. 10). The transient sea-level relevant volume shows most
variance during deglaciation, when in some relevant regions of West Antarctica, such as Siple Coast,

---

[4]https://blogs.egu.eu/divisions/cr/2018/03/23/image-of-the-week-geothermal-heat-flux-in-antarctica-do-we-really-know-anything/

grounding line migration is delayed and the local anomaly in ice thickness reaches up to 500 m. On average ice volume differse laess than 1.6 m SLE and, compared to other uncertainties discussed in this study, e.g. with regard to friction-related parameters (see next Sect. 3.4), we evaluate the choice of basal heat flux distribution of low relevance for the total ice volume history. However, in another PISM study that covers the last 2 million years with focus on ice domes, geothermal heat flux becomes the most relevant uncertain boundary condition (Sutter et al., 2019).
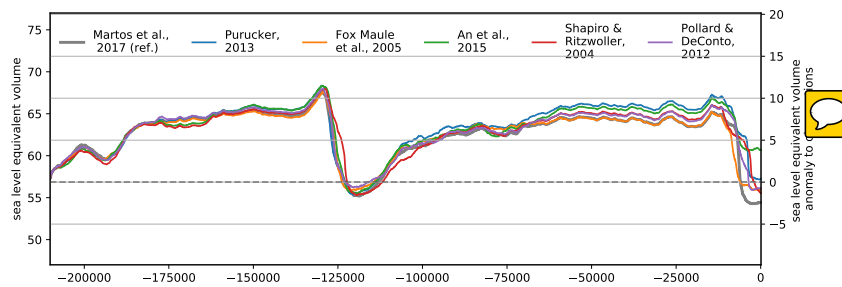
Figure 10: Simulation over two glacial cycles with different basal heat flux distributions (Martos et al., 2017; Purucker, 2013; Fox Maule et al., 2005; An et al., 2015; Shapiro and Ritzwoller, 2004; Pollard and DeConto, 2012a). Variation between the resulting ice volumes above flotation is rather small with less than 2 m SLE on average. In periods of deglaciation deviation of sea-level equivalent volume can reach more than 6 m SLE.

3.4 Basal friction

Subsurface boundary conditions are key in the understanding of Antarctic ice flow, in particular sub-glacial topography, basal morphology (e.g. presence of sediments) and subglacial hydrology (Siegert et al., 2018), ~~and how they influence basal sliding~~.

3.4.1 Pseudo plastic exponent

In PISM basal sliding is of nonlinear Weertman-type for sliding over rigid bedrock (Fowler, 1981; Schoof, 2010), where the basal shear stress $\boldsymbol{\tau}_b$ (tangential sliding) is related to the SSA sliding velocity $\boldsymbol{u}_b$ in the form

$$\boldsymbol{\tau}_b = -\tau_c \frac{\boldsymbol{u}_b}{u_0^{\,q}\,|\boldsymbol{u}_b|^{1-q}}\,, \tag{7}$$

with $0 \leq q \leq 1$ the positive sliding exponent. Value $q = 0$ represents plastic (Coulomb) deformation of the till where ice is flowing over a rigid bed with filled cavities (Schoof, 2005, 2006). Many studies use $q = 1/3$ (Schoof, 2007a; Pattyn et al., 2013; Gillet-Chaulet et al., 2016) or a linear sliding relationship between basal velocity and basal shear stress for $q = 1$, as most commonly adopted for

inversion methods (Larour et al., 2012; Gladstone et al., 2013; Yu et al., 2017). Note, that $\boldsymbol{u}_b$ results

375   from solving the non-local SSA stress balance (Bueler and Brown, 2009, Eq. 17) in which $\boldsymbol{\tau}_b$ appears as one of the terms that balance the driving stress. The PISM default sliding velocity threshold is u_0=100 m yr^{-1}.

~~Over the valid range of q we find in transient simulations a spread of reconstructed ice volumes of up to 12 m SLE (see Fig. 11),~~ while larger values lead to thinner ice sheets, in particular at interglacial

380   states. ~~We choose the pseudo-plastic q or 'PPQ' as relevant basal parameter in the large ensemble analysis in Albrecht et al. (2019).~~
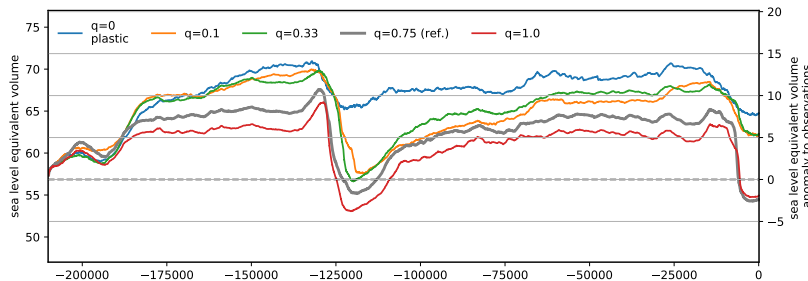
Figure 11: Antarctic ice volume history over the last two glacial cycles for different values of the basal sliding exponent q in Eq. (7). Between plastic (blue) and linear (red) ice volume above flotation can vary by up to 12 m SLE for interglacial periods, on average by 6 m SLE. Generally, smaller values of q lead to slower ice flow and hence to larger ice volumes.

3.4.2   Till properties

In our PISM simulations the Mohr-Coulomb criterion (Cuffey and Paterson, 2010) determines the yield stress τ_c as a function of small-scale till material properties and of the effective pressure N_{til}

385   on the saturated till,

$$\tau_c = \tan(\phi)\, N_{\mathrm{til}}. \tag{8}$$

~~Till~~ friction angle ϕ is a shear strength parameter for the till associated with the roughness of the bed and can be parameterized in PISM as a piecewise-linear function of bed elevation (Martin et al., 2011) assuming that marine basins and ice stream fjords have a rather loose till material, while ~~it~~

390   ~~is~~ denser in the rocky regions above the sea-level. The till friction angle is weakly confined and we assume $\phi_{min} = 2°$ in the marine basins lower than -500 m, $\phi_{max} = 45°$ above 500 m and a linear gradient between those two levels.

First, we run 50 kyr equilibrium simulations with constant boundary conditions and compare to a spatially equal distribution of till friction angle with $\phi = 30°$ (see Fig. 12). The simulation shows a

395   general overestimation of ice thickness with anomalies of more than 800 m in West Antarctica and an
overall RMSE of 372 m for the constant till friction angle. The anomalies are negative in large parts
of the East Antarctic Ice Sheet and at WAIS Divide using the piece-wise linear parameterization,
with a RMSE of about 296 m. This suggests that estimates of till friction angle in parts of the sub-
marine basins are too low, while along Siple Coast and in the Transantarctic Mountains values seem
400   too high.

These simulation results are compared with those using a till friction angle field that has been
optimized to fit the observed grounded surface elevation (or ice thickness) from Bedmap2 (Fretwell
et al., 2013), not observed velocities. We followed the simple inversion method by Pollard and De-
Conto (2012b), but we inverted for the till friction angle ϕ rather than for the basal sliding coefficient
405   τ_c. In PISM the effective pressure N_{til} in Eq. (8) is physically determined by the subglacial hydrol-
ogy model, while Pollard and DeConto (2012b) use basal temperature as a surrogate. As we run the
simulation forward in time for constant boundary conditions the till friction angle is adjusted in every
grounded grid cell every 500 years in incremental steps of $\Delta\phi$ that are proportional to the misfit to
observed surface elevation (divided by 200 m) and bounded by $-0.5° <= \Delta\phi <= 1°$. Since surface
410   elevation is underestimated in the inner parts of the East Antarctic Ice Sheet by a couple of hun-
dred meters (eventually due to underestimated accumulation), retrieved till friction angles reaches
the maximum value of $\phi_{i_{max}} = 70°$ which enhances yield stress by about an order of magnitude.
In contrast, in Siple Coast the minimum values of $\phi_{i_{min}} = 2°$ compensates for overestimated ice
thickness (see lower rows in Fig. 12). Thus, the RMSE of ice thickness can be significantly reduced
415   to 141 m (or even 123 m for $\phi_{i_{min}} = 0.5°$) and the modeled ice volume is only 0.5% below observa-
tion. The retrieved distributions of till friction angles are rather independent of initial conditions and
iteration parameters (not shown here). But this method may overcompensate for inconsistent model
boundary conditions or not adequately represented processes.
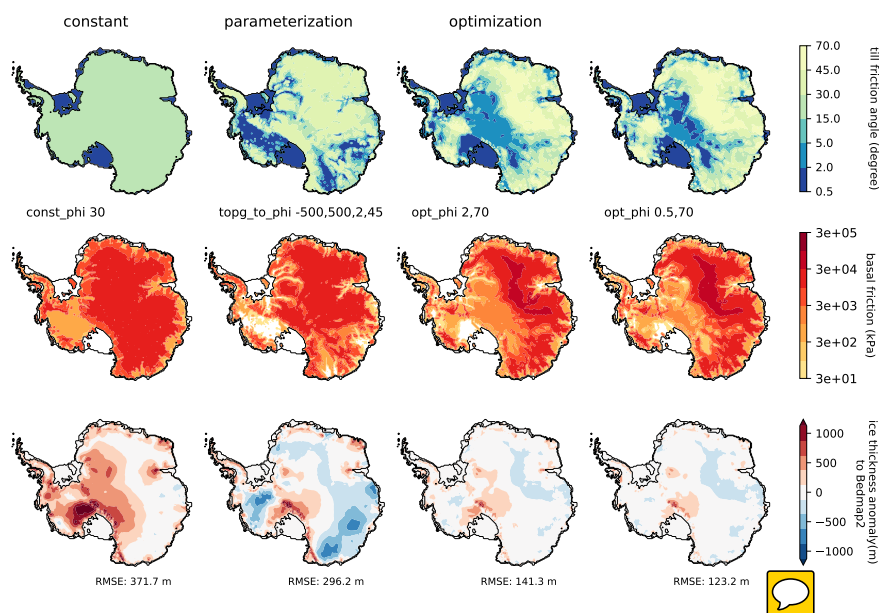
Figure 12: PISM equilibrium simulations for different basal friction fields (τ_c in middle row) based on different till friction angle distributions (ϕ in first row). First column with spatially uniform till friction angle of $30°$, second column show till friction angle according to PISM parameterization as function of bed topography, last columns using a simple inversion technique with different minimal $\phi_{i_{min}}$. Last row shows the resulting ice thickness anomaly to Bedmap2 observations (Fretwell et al., 2013) with improvements particularly in East Antarctica and Siple Coast region and overall RMSE reduced to 123 m (with parameters ESIA=1 and $C_d = 5\,\text{mm/yr}$).

For the transient response of the ice sheet's volume to the different distributions of till friction an-
420 gle, we find similar glacial ice volumes for the depth-dependent parameterization and the optimiza-
tion, while in contrast interglacial ice volumes differ considerably (cf. orange and grey in Fig. 13).
For the spatially constant till friction angle of $30°$ underneath the grounded ice sheet and $2°$ on the
ocean floor, we simulate similar glacial cycle volume histories as for the parameterizations (blue). In
fact, we find a larger shift in ice sheet volume for variations of till friction angle on the ocean floor.
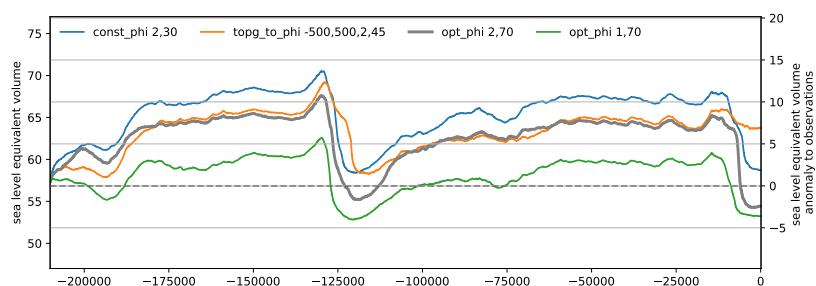
Figure 13: Ice volume histories over two glacial cycles for different parameterizations of till friction angle. Volumes at Last Glacial Maximum are similar for same $\phi_{min} = 2$ in the marine ice sheet sections, but deglaciation is omitted in the depth-dependent parameterization (orange). For a smaller $\phi_{min} = 1$ we find generally smaller ice volumes, as discussed in the next section.

425 **Till properties under modern ice shelves**

Friction (and also bed topography) at the ocean bed underneath the modern ice shelves is weakly constrained, as the optimization algorithms only applies to modern grounded regions (e.g., Pollard and DeConto, 2012b; Morlighem et al., 2017). Friction coefficient on the continental shelf has been thus chosen as one of the ensemble parameters in Pollard et al. (2016, 2017). In PISM the till friction

430 angle accounts for the flow properties of the substrate and enters the yield stress definition ==with its tangent== (see Eq. (8)). As sandy sediments are prevalent in the ice shelf basins low values of ϕ are likely (Halberstadt et al., 2018). ~~On the other hand,~~ till friction angle in the ice shelf basins is a crucial parameter, which determines the thickness of the extended ice sheet for LGM conditions and hence the potential contribution to the global sea-level change.

435 Modeled LGM ice volumes increase by up to 2–4 m SLE per 1° change in minimal till friction angle (see Fig.14). Compared observations we detect much higher volumes above flotation at present-day for $\phi_{min} \geq 3°$. At the same time, relative volume changes ~~from~~ LGM ~~to~~ modeled modern state become slightly smaller for rougher basins. This effect may be related to the effect of friction on the rate of grounding line retreat. The spread of ice volumes among the four experiments with

440 $\phi_{min} = 1–5°$ is on average 13 m SLE. ~~For now we~~ chose as a reference a lower bound for the till friction angle of $\phi_{min} = 2°$ in ocean regions, as simulated deglaciation shows a good match to modern ice volume (Fig.14, grey).
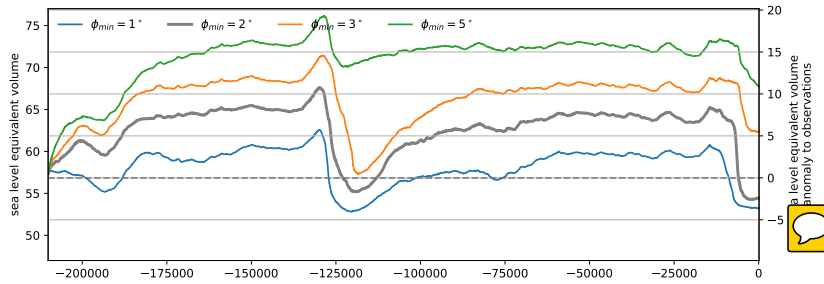
Figure 14: Simulation of two glacial cycles for different minimal till friction angles in the marine sectors. The choice of $\phi_{\min}$ has strong influence on the reconstructed ice volume at glacial maximum, with high till friction angles leading to more friction and hence thicker ice sheets. Within the plausible range from $1.0°$–$5.0°$ we find up to 18 m SLE difference in ice volume above flotation, on average 13 m SLE.

3.4.3 Subglacial hydrology

Friction at the ice sheet base is weakly constrained. A time-dependent basal substrate rheology scheme allows meltwater generated at the ice-sheet bed to saturate and weaken the subglacial till layer (de Fleurian et al., 2018). The resulting reduced basal traction allows grounded ice to accelerate. This can, in turn, cause dynamic thinning, a reduction in driving stress and ultimately a reduced ice stream flow later on. In PISM yield stress is defined as Mohr-Coulomb criterion (Cuffey and Paterson, 2010) as in Eq. (8), with the hydrology-related effective pressure

$$N_{\text{til}} = N_0 \left(\frac{\delta P_0}{N_0} \right)^s 10^{(e_0/C_c)(1-s)}, \tag{9}$$

which accounts for the overburden pressure $P_0 = \rho_i g H$ for given ice thickness H, and the fraction of effective water thickness in the till layer s, while all other parameters are constants (adopted from Bueler and van Pelt, 2015).

Till water distribution

Till water in our PISM simulations is modeled as boundary layer with an effective thickness of water content W with respect to a maximum amount of basal water $W_{\text{til}}^{\max} = 2\,\text{m}$ and enters as fraction s in Eq. (9). We use a non-conserving hydrology model that connects W_{til} to the basal melt rate M_b, where ρ_w is the density of water and C_d is a fixed drainage rate,

$$\frac{\partial W_{\text{til}}}{\partial t} = \frac{M_b}{\rho_w} - C_d. \tag{10}$$

PISM's default drainage rate of 1 mm/yr is smaller than the basal melting in most of the grounded Antarctic Ice Sheet regions, such that till saturates over time. Higher decay rates can effectively drain

the till water in the inner ice sheet regions which generally cause less extended and more confined
ice streams, less ice discharge and hence thicker ice sheets. In transient glacial cycle simulations, this
relationship applies for both present-day climate conditions (see Fig. 15) and for colder-than-present
465   climates. A till water drainage rate of 10 mm/yr can cause up to 11 m SLE additional ice volume
(orange line in Fig. 16).
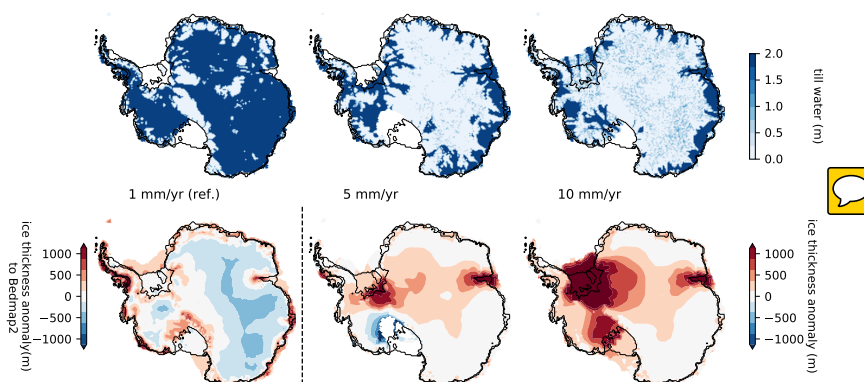
Figure 15: Present-day result of glacial cycle simulation showing ice thickness anomaly to Bedmap2
(lower left) and to reference (lower right) for different till water decay rates (1 mm/yr left, 5 mm/yr
middle and 10 mm/yr right column) causing different till water distributions underneath the ice
sheet (upper row). For a decay rate of 1 mm/yr about 90% of ice sheet's bed is saturated, while for
10 mm/yr saturated till is only found in the coastal regions and underneath fast-flowing ice stream.

Another relevant aspect is the initial till water fraction on ocean beds that become grounded.
PISM assumes that grounding line advances into dry till area $W_{til} = 0$, where a till water layer can
form over the following decades or centuries. If we assume a rigid till layer instead with $W_{til} =$
470   W_{til}^{max} for an advancing grounding line we find slower growth of glacial ice sheet volume and much
earlier deglaciation, while ice volumes are comparable to the reference case for present-day climate
conditions (compare green and grey line in Fig. 16).
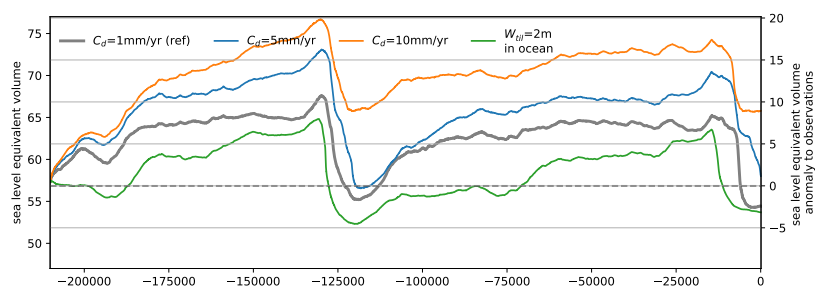
Figure 16: Simulation over two glacial cycles for different till water decay rates underneath the grounded ice sheet. Higher values cause less extended ice streams, less ice discharge and hence thicker ice sheets (blue and orange). If we assume maximum till water fraction across ocean beds, grounding line advance of marine glaciers is decelerated. Accordingly, we find less extended and thinner ice sheet at glacial periods, earlier retreat but similar present-day results, compare grey and green lines.

Overburden fraction

The effective pressure cannot exceed the overburden pressure, i.e., $N_{\mathrm{til}}^{\max} = P_0$ (for details see Bueler and van Pelt, 2015, Sect. 3.2), while in the case of saturated till layer ($s = 1$) we find a lower limit $N_{\mathrm{til}}^{\min} = \delta P_0$, with δ ~~a certain~~ fraction of the effective overburden pressure (PISM default is $2\,\%$, our reference is $4\,\%$), at which the excess water will be drained into a transport system. As in large portions of the grounded Antarctic Ice Sheet, where a certain amount of till water is abundant, the parameter δ ~~practically~~ scales the lower bound of the yield stress and hence affects the total ice volume above flotation considerably. For a doubling in δ, PISM simulations suggest almost a doubling in glacial ice volume change (see Fig. 17). Also, for higher values of δ, the onset of deglaciation occurs earlier.
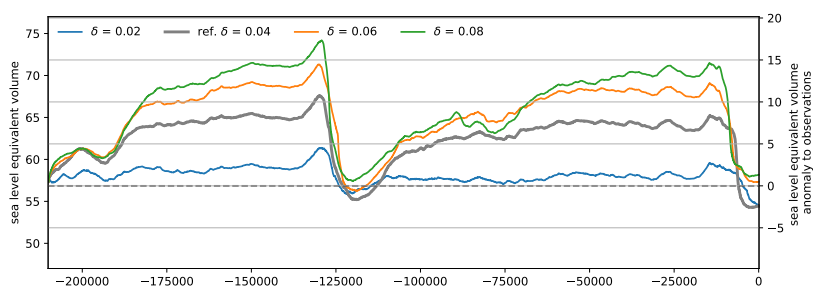
Figure 17: Volume above flotation in simulation over two glacial cycles for different values of the overburden pressure fraction parameter δ in Eq. (9). This parameter has strong influence on the reconstructed ice volume, particularly at glacial maximum, with high parameter values leading to more friction and hence thicker ice sheets. For the evaluated range of 2–8% we find up to 12 m SLE difference in ice volume above flotation.

4 Climatic forcing

In our PISM simulations the Antarctic Ice Sheet responds to externally prescribed climatic forcings.
485   In this section we choose reconstructions of Antarctic temperatures and sea-level variations which implicitly incorporate the past climate response to changes in orbital configurations and atmospheric CO_2 content. However, in this stand-alone mode no feedbacks of the ice sheet to the climate system are considered, but we discuss contributions of the climatic forcings to the volume evolution of Antarctic Ice Sheet.

490   ### 4.1 Sea-level forcing

The Antarctic Ice Sheet, particularly in its western part, rests on a bed below the sea-level with floating ice shelves attached. The location of the grounding line in PISM is solely determined by the flotation criterion (cf. $H \leq h_f$ in Eq. (2)) and ~~therewith~~ also by the current sea level z_{sl}, for given ice thickness H and bed elevation b. Glacial dynamics in the marine ice sheet sections are
495   hence sensitive to changes in sea-level, which has been 120–140 m lower than today at the Last Glacial Maximum. We neglect regional sea-level effects due to changes of the rotation of the earth or due to self-gravitation, which can have a stabilising effect on the ice sheet locally (Konrad et al., 2015). Instead we consider global mean sea-surface heights reconstructions prescribed by the ICE-6G_C GIA model, which includes the influence of the changing surface area of the oceans (Stuhne
500   and Peltier, 2015, 2017, courtesy Dick Peltier). To analyse the sensitivity of the model's response to the choice of the sea-level forcing we compare ~~also~~ to a few other reconstructions by Lambeck et al. (2014); Bintanja and Van de Wal (2008); Imbrie and McIntyre (2006); Spratt and Lisiecki

(2016). Focusing on the last deglacial period the timing of sea-level rise onset in response to the melting of the northern hemispheric land ice masses varies by a couple of thousand years among the

505 different sea-level curves (Fig. 18), e.g. the reconstruction from a glacio-isostatic adjustment model simulation of eustatic sea level by Stuhne and Peltier (2015) peaks already before 25 kyrs BP with around -130 m below present (blue) while the much smoother SPECMAP sea-level curve by Imbrie and McIntyre (2006) has a minimum around -18 kyr BP and a comparably late relaxation to the present-day sea-level ~~stand~~ (orange).

510 The modeled Antarctic Ice Sheet response at Last Glacial Maximum is rather unaffected by the choice of the sea-level forcing, while at present-day ice volume varies by up to 2.5 m sea-level equivalent (lower right panel of Fig. 18). In particular the so-called meltwater pulse 1a (MWP1a Liu et al., 2016) around 14.35 kyr BP with a global sea-level rise of 9–15 m or more within a few hundred years (see grey vertical band in Fig. 18) is well represented as step in the sea-level curve

515 in the reference forcing time series of the ICE-6G_C (VM5a) model. This triggers a comparably early and quick grounding line retreat in the Ross and Weddell Sea embayment, where the large ice shelves become afloat.
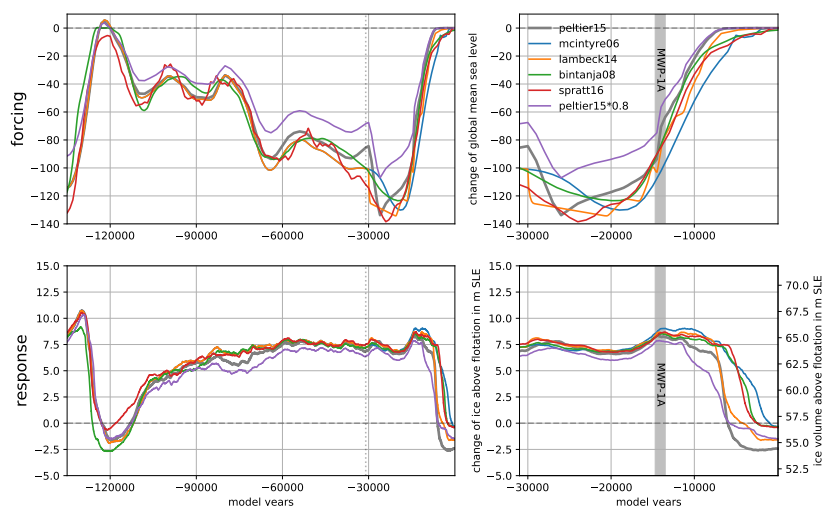
Figure 18: Time series of reconstructed sea-level change over the last 135 kyr (upper left) and the last 30 kyr (upper right) by Stuhne and Peltier (2015); Imbrie and McIntyre (2006); Lambeck et al. (2014); Bintanja and Van de Wal (2008); Spratt and Lisiecki (2016) and corresponding PISM-simulated sea-level relevant ice volume anomaly relative to observations (Fretwell et al., 2013) in lower panels. In order to approximate the effect of self-gravitation we scaled the ICE-6G forcing (Stuhne and Peltier, 2015) by 80%. For about 25 m higher sea-level stand at LGM we find almost the same modeled ice volume, while we find much earlier and more gradual deglaciation.

If self-gravitational effects were accounted for within a sea-level model, the local sea-level anomaly at the grounding line would be reduced compared with the global mean. A scaling of the sea-level forcing by 80–90% would mimic the first-order feedback of self-gravitation on grounding line motion. Interestingly, neither the ice volume at LGM nor at present-day is significantly affected, but the onset and rate of deglaciation (Fig. 18, purple line).

4.2 Surface temperature forcing

Varying surface temperatures drive ice flow changes on glacial timescales. In PISM we model the non-linear thermo-coupling via a Glen-type flow law with a generalized form of Arrhenius form. More specific, PISM's default is the polythermal Glen-Paterson-Budd-Lliboutry-Duval law (Lliboutry and Duval, 1985; Aschwanden et al., 2012), where the ice softness depends on both the temperature and the liquid water fraction, so it parameterizes the (observed) softening of pressure-melting-temperature ice as its liquid fraction increases. Since vertical diffusion processes in the ice

530   are rather slow, the corresponding response of the ice sheet to surface temperature anomalies occurs
with some delay of up to a few thousand years, involving a long-lasting memory for past events (see
Sect. 5.1.

On paleo time scales PISM can use temperature reconstructions from ice cores based on deuterium
isotopes, such as the EPICA Dome C (EDC, Jouzel et al., 2007) with a well resolved timeseries

535   over the last 803 kyr (EDC3 age scale), representative for the inner East Antarctic Ice Sheet. How-
ever, most of the ice-dynamical changes on glacial timescales occur in the marine regions of the
West-Antarctic Ice Sheet, ~~whereas~~ the much closer WAIS Divide ice core provides a highly resolved
temperature reconstruction (WDC, Cuffey et al., 2016), which spans only the last 67.7 kyr. As sur-
face temperature forcing $\Delta T(t)$ we consider the temperature anomaly with respect to the year 2000

540   A.D. added to the parameterized temperature field of Sect. 3.1. For model periods before 67.7 kyr
the temperature anomaly of EDC applies (with respect to the last 1000-years average), see upper
panels in Fig. 19.

As WDC temperature rise occurred somewhat earlier than at EDC the Antarctic Ice Sheet responds
with higher deglaciation rate (cf. grey in blue line). Comparisons with other ice core temperature

545   reconstructions, however, suggest a superimposed effect of surface height change during deglaciation
at WDC (Werner et al., 2018). In addition, Antarctic temperature anomalies at glacial maxima with
up to -10 K may be overestimated systematically (personal communication Eric Steig). We also test
for a scaled temperature reconstruction from WDC with LGM temperature of only 6 K below present
(see orange lines in Fig. 19). Interestingly, weaker temperature forcing results in slightly thicker

550   glacial ice volume (probably an effect of temperature-coupled surface mass balance, see Sect. 4.4)
and delayed deglaciation.
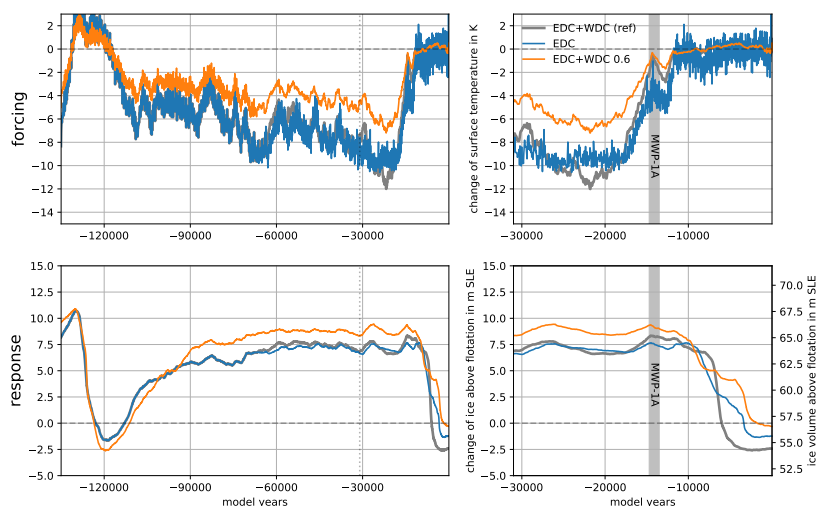
Figure 19: Timeseries of PISM-simulated ice volume above flotation relative to observations (Fretwell et al., 2013) over last 135 kyr (lower left) and last 31 kyr (lower right) forced with three different surface temperature reconstructions (upper panels) at WDC (Cuffey et al., 2016) and EDC (Jouzel et al., 2007) leading to different ice volume histories, particularly during deglaciation period. WDC temperature reconstruction scaled by 60% cause 2 m SLE larger glacial ice volume and slower deglaciation.

4.3 Ocean temperature forcing

Sub-shelf melting in PISM is calculated via PICO (Reese et al., 2018) from salinity and temperature in the lower ocean layers on the continental shelf (Schmidtko et al., 2014) averaged over 18 sep-
555 arate basins adjacent to the ice shelves around the Antarctic continent. While salinity change over time in the deeper layers is neglected in this study, the ocean temperature responds with some delay to changes in the global mean temperature. We analyzed simulations with coupled climate model ECHAM5/MPIOM over more than 6,000 years following a four-fold increase in CO_2 forcing (courtesy Li et al., 2012) and identified the anomaly in global mean temperature, in Antarctic temperature
560 (south of 66° S) and in Antarctic ocean temperature at depth levels between 500 and 2,500 m. After the response time of about 3,000 years the ocean temperature stabilizes at about $f_o = 0.75$ of the global mean anomaly, while Antarctic surface temperature anomaly is amplified by a factor of 1.8 (see Fig. 20). As we intend to estimate ocean temperature change from ice surface temperature change reconstructed from ice cores, we could fit the response function directly from the Antarctic

565 mean surface temperature in the climate model data. But we found that, ~~for considered time scales~~, Antarctic surface temperatures respond rather linearly with global mean temperature change (and respective amplification factor). In addition, ~~as~~ response to global mean temperature, we build on a more general definition, which is easier to compare to other approaches.
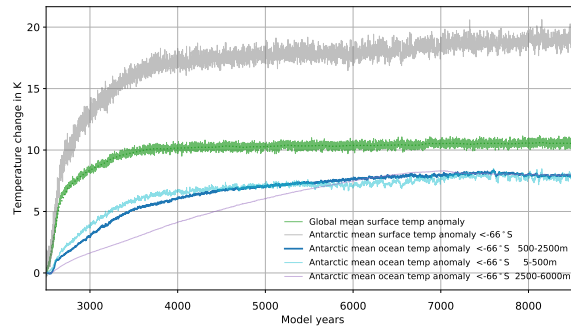
Figure 20: Global mean temperature (green), Antarctic mean temperature south of 66°S (grey) and ocean temperature averaged over upper 500m (light blue), intermediate (500-2500m, blue) and deeper layers (below 2500m, violet) of the MPIOM model coupled to ECHAM5 forced by a CO_2 quadrupling within 140 years (Li et al., 2012).

Using linear response theory (Winkelmann and Levermann, 2013) and assuming the global mean
570 temperature anomaly $\Delta T_{GM}(t)$ via a convolution integral related to the ocean temperature as

$$\Delta T_o(t) = \int_0^t dt' \, R(t - t') \, \Delta T_{GM}(t'), \qquad (11)$$

we reconstruct a response function $R(t)$ and a corresponding fit function with $R^*(t) \sim t^{-\alpha}$ (see Fig. 21), which vanishes beyond the typical response time τ_r. For $\alpha = 2$ and with integration constant in the numerator yielding unit integral, such that

575 $$\int_0^{\tau_r} R^*(t) \, dt = f_o, \qquad (12)$$

this yields

$$R^*(t) = f_o \cdot \frac{[t_0^{-1} - (\tau_r + t_0)^{-1}]^{-1}}{(t + t_0)^2}, \qquad 0 \le t \le \tau_r. \qquad (13)$$

.
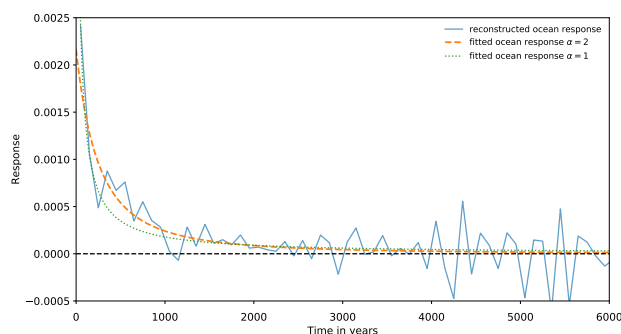
Figure 21: Reconstructed noisy response function $R(t)$ (blue) with fitted function $R^*(t)$ (orange dashed) as in Eq. 13. For comparison fit function with $\alpha = 1$ (green dotted).

The inferred response fit function convoluted with a given timeseries of global mean surface tem-
580 perature anomaly (or here with the scaled ice core temperature reconstruction) hence provides an
estimate for the corresponding change in ocean temperature at intermediate depth. Figure 22 shows
the estimated ocean temperature anomaly curve (blue) with some delay with respect to the WDC sur-
face temperature reconstructions (Cuffey et al., 2016, , grey), here scaled by $0.75/1.8 = 5/12 = 42\%$
(purple). WDC likely ~~reflects better~~ the ocean conditions in the ~~widely~~ marine West Antarctic Ice
585 Sheet than the EDC in central East Antarctica (Jouzel et al., 2007). The resulting timeseries is com-
parably smooth with a resolution of 500 years and serves as PICO ocean temperature forcing. As
negative ocean temperature anomalies can result in unphysical values below pressure melting point,
we leave it to the PICO module to assert this lower bound, such that melting vanishes and overturning
circulations halts accordingly. As a consequence ocean forcing is not relevant for much colder-than
590 present glacial climates.
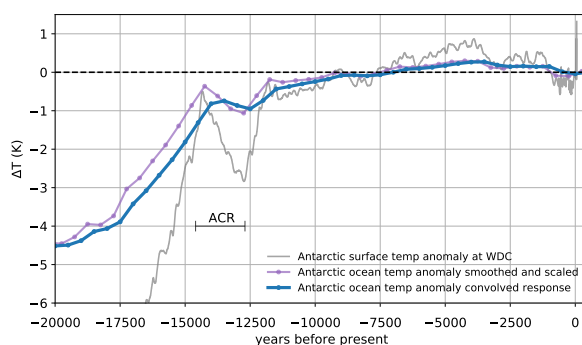
Figure 22: Response of the intermediate ocean temperature (blue) to surface temperature anomaly as reconstructed from WDC (Cuffey et al., 2016, grey line) assuming a polar amplification factor of 1.8 and an equilibrium ocean scale factor of 0.75 as identified in climate model analysis for a warming scenario. Convolution yields a delayed response with respect to the forcing (compare violet and blue curve). Dots indicate bins of 500 year means. The timeseries includes the Antarctic Cold Reversal (ACR) 14.6-12.7 kyr BP (Fogwill et al., 2017).

Transient PISM simulations reveal effects of ocean temperature forcing on the timing of deglaciation with delays of a few thousand years when compared to the scaled surface temperature forcing timeseries (Fig. 23). When we apply ~~directly~~ the smoothed and scaled surface temperature forcing as PICO forcing we still get very similar results, but a slightly earlier retreat (green). Simulations

595 reveal that the power of the response function (cf. Fig. 21) is of minor relevance for the ice sheet's response (compare grey and blue lines), and so is the amplitude of cooling at glacial stage, here scaled by 60% (red). If the ocean forcing is related to the EDC temperature reconstruction (see previous Section 4.2) we find a later warming and hence a delayed deglaciation (orange). ~~As the forcing is defined as anomaly,~~ which ~~vanished towards~~ present day, the modeled modern ice sheet config-

600 urations are rather independent of ocean temperature forcing ~~applied~~. However, response functions require linearity, causality and stationarity. There is literature suggesting periods of decoupled ocean and surface temperature evolution (e.g. Antarctic Cold Reversal) with strong potential effects on the ice sheet deglaciation, which is discussed in Sect. 5.2.
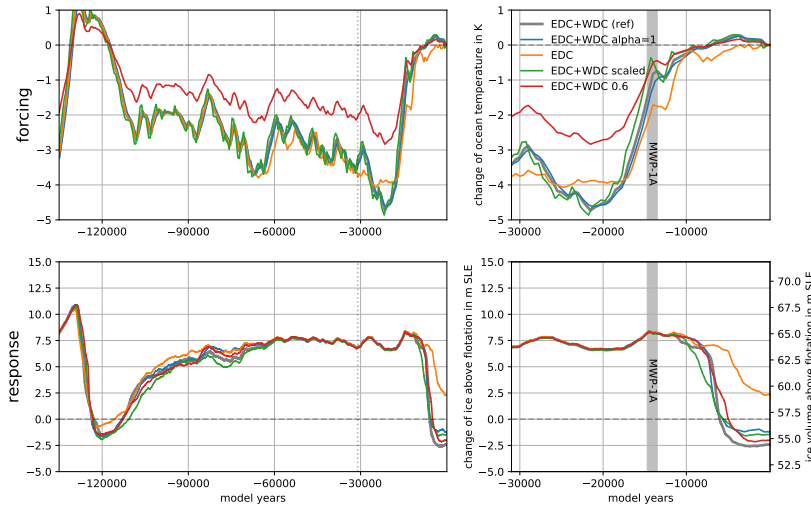
Figure 23: Sensitivity of transient ice volume above flotation to varied ocean temperature forcing. Reference simulation (grey) is based on EDC+WDC surface temperature with fit response function of power $\alpha = 2$. The resulting ice volume change is similar for a fit response function with power $\alpha = 1$ (blue). Even if ocean temperature forcing responds immediately to surface temperature anomalies (green) the resulting effects on ice volume are comparably small. If different surface temperature reconstructions are used from EDC with $\alpha = 2$ (orange), we find for later warming delayed deglaciation accordingly. If the amplitude of WDC surface temperature anomalies was 40% lower (red), this would have only negligible effect on the modeled ice volume.

4.4 Precipitation forcing

605 Continental-scale precipitation change is closely related to temperature change. While colder temperature lead to slower ice flow and hence larger ice masses, they also lead to dryer conditions and hence to less ice mass accumulation. This effect is based on the Clausius-Clapeyron-relationship which suggests higher atmospheric moisture capacity and hence more accumulation in a warmer atmosphere. Analysis of ice core and modeling data suggest for the Antarctic continent a linear scaling

610 relationship of $f_{p,l} = 5 \pm 1\,\% \, K^{-1}$ precipitation change per degree continental average temperature change (Frieler et al., 2015). In PISM simulations, precipitation forcing $P(t)$ is coupled directly to the temperature forcing $\Delta T(t)$ (Sect. 4.2) using an exponential relationship (Ritz et al., 1996; Quiquet et al., 2012, Eq. 2), which scales the present-day mean precipitation field P_0 as

$$P(t) = P_0 \exp\left(f_p \, \Delta T(t)\right) \approx P_0 \left(1.0 + f_{p,l} \, \Delta T(t)\right). \tag{14}$$

615   The exponential function is hence compatible with the precipitation lapse correction (Eq.(6)) and
it allows for easier comparisons with other studies that use power law relationships, e.g. with $f_p =$
$\ln(2)/10$ for Pollard and DeConto (2009). In fact, precipitation change is depending very much on
the Antarctic region. In our simulations we use ~~for $\Delta T(t)$~~ a combination of temperature reconstructions from the EDC and WDC (see Sect. 4.2), for which the study by (Frieler et al., 2015) suggest

620   slightly higher values of $f_{p,l} = 5.9 \pm 2.2\,\% \, K^{-1}$ and $f_{p,l} = 5.5 \pm 1.2\,\% \, K^{-1}$, respectively. In East
Antarctica values are even slightly higher than in West Antarctica.

     In glacial periods with much colder temperatures of $\Delta T = -10\,K$, an exponential precipitation
change with $f_p =$ 7–9% K^{-1} yields 50–60% less precipitation as compared to modern times. Without any precipitation change our simulations suggest up to 7 m SLE thicker ice sheets at glacial

625   maximum (cf. orange and blue line in Fig. 24). The reference value of 7% K^{-1} precipitation change
corresponds to more than 50% dryer conditions than present and about 3–4 m SLE less ice volume
than for 5% K^{-1} (cf. blue and grey line).

     ~~There are also~~ reconstructions of precipitation at ice core sites ~~available~~, e.g. at WDC (Buizert
et al., 2015; Fudge et al., 2016), ~~which reveals~~ precipitation ~~change~~ relative to present of up to -

630   60% during glacial maximum and up to 25% more precipitation through the Holcene. Figure 24
shows the corresponding transient effects of reconstructed precipitation forcings on the ice sheet's
volume above flotation. The excess accumulation prohibits deglaciation and causes a more than
10 m SLE larger modern ice sheet configuration. However, the reconstructed signal may be biased to
some extent from a lapse-rate effect due to surface elevation changes during deglaciation (personal

635   communication Eric Steig). We hence choose 'PREC' as relevant climate forcing parameter in the
large ensemble analysis in Albrecht et al. (2019).
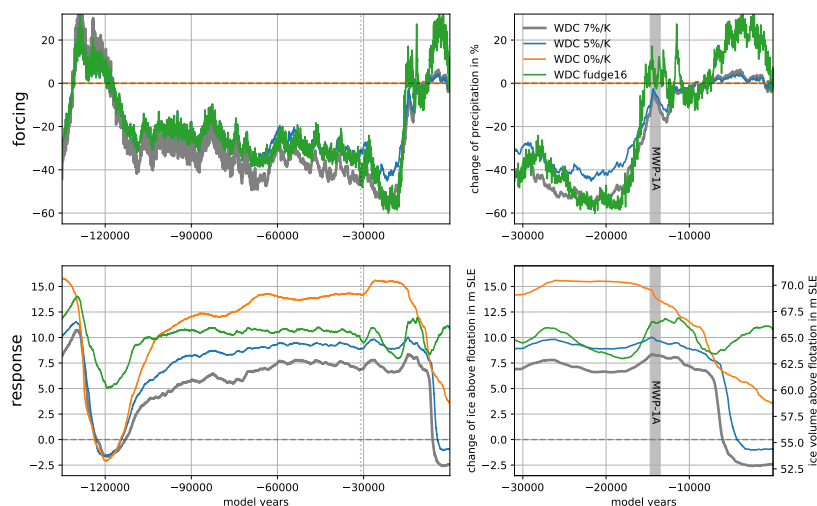
Figure 24: Sensitivity of transient ice volume above flotation to varied precipitation forcing. Grey curve is the reference with an exponential scaling factor of $7\%\,\mathrm{K}^{-1}$ with respect to WDC temperature reconstruction (Cuffey et al., 2016). Ice volume is slightly larger for $5\%\,\mathrm{K}^{-1}$ (blue) and much larger without precipitation forcing (orange). Deglaciation is prohibited when using WDC accumulation reconstruction (Fudge et al., 2016) with additional accumulation during Holocene (green).

4.5 Combined effects of climatic forcings in glacial cycle simulations

In our simulations with PISM the above described climatic forcings (Sections 4.1–4.4) have different effects on the Antarctic Ice Sheet evolution at different periods. Both, temperature and sea-level

640   forcing reveal a signature not only of the dominant 100 kyr orbital cycle period, but with smaller amplitudes also of the higher-frequency cycles, e.g. MIS 3 around 57 kyr BP (Weichselian High Glacial) or the Last Glacial Maximum MIS 2 around 29 kyr BP (Lisiecki and Raymo, 2005). For glacial cycle simulations, sea-level forcing has the strongest effect on the ice volume, as it alone triggers larger glacial ice volume than in the reference simulation (see Fig. 25b, orange and grey).

645   However, the rising sea-level during deglaciation alone induces only little ice sheet retreat. When sea-level forcing is turned off, the other forcings balance each other such that ice volume remains approximately at modern level through glacial periods (Fig. 25c). Also surface temperature forcing (blue) alone can produce glacial volumes of similar extent as sea-level forcing. ~~But if~~ surface temperatures ~~stay~~ at modern level, the other forcings can still produce a glacial maximum volume that is

650   only 3 m SLE lower than the reference. In our simulations, surface temperature anomalies also drive

changes in ocean temperature and precipitation. Ocean temperatures forcing has only little effect on glacial extent, but it influences the onset of deglaciation (red). Without ocean forcing the interglacial (and modern) ice volume is up to 7 m SLE larger than the reference (Fig. 25c). While sea-level and temperature forcings cause a growth of ice sheets at glacial climates, precipitation forcing has an op-

655 posite effect (Fig. 25, green). Without precipitation the Antarctic Ice Sheet can reach glacial extents of up to 7 m SLE above the reference (coupled to the surface temperature forcing with $f_p = 7\%/K$). This result of the precipitation forcing for glacial climates also explains why the individual responses to the sea-level and the surface temperature forcing exceed the reference ice volume by about 3-4 m SLE, in which all four forcings are superimposed. The simulations hence suggest that the precipita-

660 tion scaling parameter f_p is highly relevant for the ice sheet's extent at glacial maximum and will be considered as ensemble parameter 'PREC' in Albrecht et al. (2019).
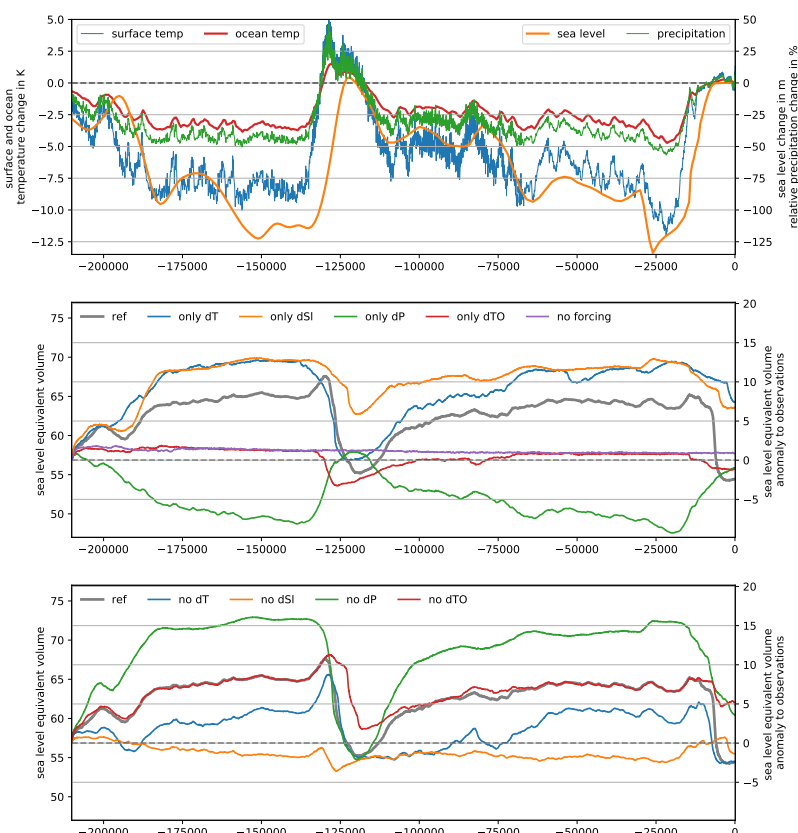
Figure 25: Antarctic Ice Sheet volume above flotation for combination of surface temperature, ocean temperature, sea-level and precipitation forcings (upper panel) as defined in previous sections. Middle panel shows the ice sheet's response to individual forcings (or constant equilibrium conditions in purple), while in lower panel one forcing is off as compared to the reference simulation (with all forcings combined, in grey). Sea-level forcing (orange) and surface temperature forcing (blue) have the strongest effects: each alone can cause larger glacial ice volume than in the reference simulation. Yet, each alone cannot initiate effective glacial retreat during for modern climate. In contrast, ocean temperature forcing (red) has no effect on glacial volume but it amplifies deglaciation. Precipitation forcing (green) counteracts sea-level and temperature forcings at glacial climates.

Table 1: Physical constants and parameter values.

Parameter	Value	Units	Physical meaning
ρ_i	910	kg m^{-3}	Ice density
ρ_o	1028	kg m^{-3}	Seawater density
ρ_w	1000	kg m^{-3}	Water density
g	9.81	m s^{-2}	Gravitational acceleration
A_o	3.61×10^{14}	m^2	Surface area of world ocean
c_a	$2.2–2.7 \times 10^8$	m^2	Projected grid cell area for 16 km resolution
f_o	0.75		Amplification factor ocean to global mean temperature
f_s	1.8		Amplification factor Antarctic to global mean temperature
τ_r	3000	yr	Typical response time in intermediate ocean temperature
K	$1\text{-}100\ (10) \times 10^{16}$	m s	Eigencalving constant
H_{cr}	0–225 (75)	m	Thickness calving threshold
n	2–4 (3)		Exponent in Glen's flow law
E_{SSA}	0.3–1.0 (0.6)		Enhancement factor for SSA stress balance
E_{SIA} (ESIA)	1–7 (2)		Enhancement factor for SIA stress balance
f_p (PREC)	2–10 (7)	% K^{-1}	Relative precipitation change with air temperature
η (VISC)	$1–100\ (5) \times 10^{19}$	Pa s	Earth upper mantle viscosity
D	$5–100\ (50) \times 10^{23}$	N m	Flexural rigidity of lithosphere
ϕ	1–70	°	Till friction angle
$\phi_{\min}$	0.5–5 (2)	°	Minimal till friction angle in marine parts
q (PPQ)	0–1 (0.75)		Basal friction exponent in Eq. (7)
u_0	100	m yr^{-1}	Threshold velocity in sliding law Eq. (7)
N_0	1000	Pa	Reference effective pressure
δ	0.02–0.1 (0.04)		Parameter determining effective overburden pressure δP_0
e_0	0.69		Reference void ratio at N_0
C_c	0.12		Till compressibility
$W_{\max}$	2	m	Maximum water thickness in till
C_d	0.001–0.01 (0.001)	m yr^{-1}	Till drainage rate
b		m	Bed elevation
H		m	Ice thickness
z_{sl}		m	Sea level anomaly
τ_c		Pa	Yields stress

5 Perturbation experiments

5.1 Energy spin-up procedure and intrinsic memory

In the introduction to PISM (Sect. 1.1) we have briefly described a spin-up procedure, which results

665 in a three-dimensional enthalpy field that is in balance with the modern climate boundary conditions (see Sect. 3). We assume hereby that present-day conditions have been similar to those in the penultimate interglacial (210 kyr BP). As the three-dimensional enthalpy field carries the memory of past climate conditions, a more realistic spin-up climatic boundary condition may be achieved when the temperature reconstruction of the previous glacial cycles (EDC, see Sect. 4.2) or the long-

670 range mean is used as anomaly forcing, while the ice sheet geometry remains fixed at present-day observations (Bedmap2; Fretwell et al., 2013). Here we investigate to what extent the choice of the temperature forcing in the enthalpy field spin-up can affect subsequent full-dynamics simulations over the last two glacial cycles until present.

Simulations are conducted with identical model settings and climate forcing but different initial

675 energy states. The modeled ice volumes converge at glacial maxima with less than 0.2 m SLE difference among the three simulations. As deglaciation can be delayed by a few thousand years modern ice volume can differ by up to 2 m SLE (see Fig. 26 around time 0 BP). Also the full-physics spin-up over four glacial cycles reveals comparable differences to the reference (Fig. 28). In order to evaluate to what extent the sensitivity of the simulation results to changes in the energy initialization method

680 is related to a memory effect (that should vanish) or to deterministic chaos, we continues the simulations for the same glacial climate forcing (but now different geometries), such that simulations ran for 420 kyr and 630 kyr in total. Interestingly, simulated ice volumes diverge to some extent during interglacial states. As deglaciation reveals nonlinear threshold behavior it can amplify small differences at glacial maxima. Ice thickness variations of up to 1000 m are found mainly in the large ice

685 shelf basins of Ross (Siple Coast), Amery and Ronne-Filchner (Bungenstock), ~~see Fig. 27~~, mostly determined by the location of the migrating grounding line. Hence, the remaining deviations can be interpreted as model-internal uncertainty and should be kept in mind when comparing and evaluating ensembles of Antarctic ice volume reconstructions. Comparably small differences in initial conditions could be also related to numerical settings, such as number of CPU.
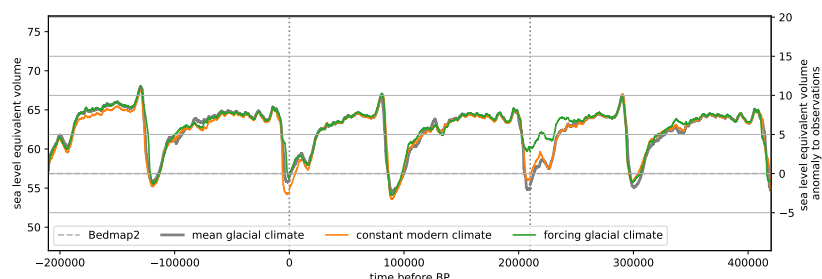
Figure 26: Simulations over two last glacial cycles (repeated three times in a row, indicated by vertical dotted lines) with identical parameter settings but based on different spin-up procedures with prescribed initial ice sheet geometry, in which the three-dimensional ice enthalpy field (and basal melt pattern) adjusts to climatic boundary conditions. ~~In grey~~ initialization method as used in reference simulations.
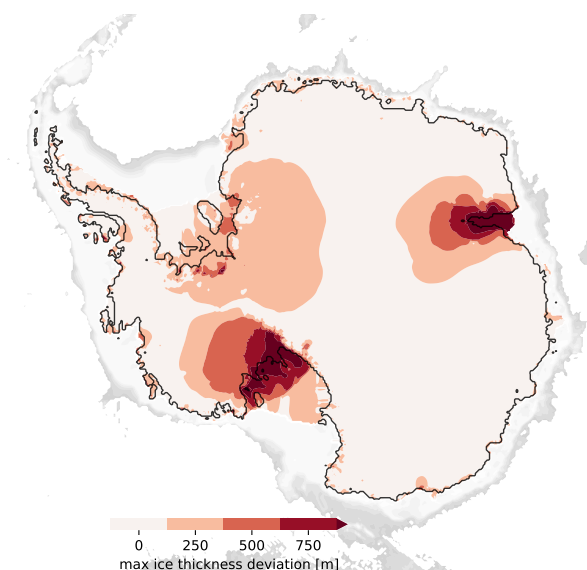
Figure 27: Present-day maximum ice thickness difference of three simulations after three rounds of two-glacial-cycle simulations with identical model settings, but for different initial enthalpy states (cf. final state in Fig. 26). In particular Siple Coast and Amery trough show ~~most~~ variations of more than 1 km ice thickness.
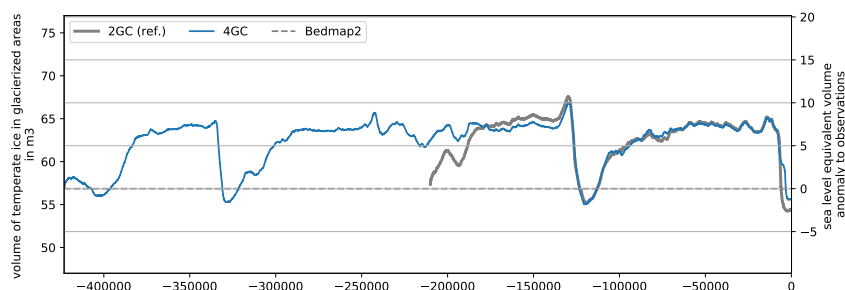
Figure 28: Simulation over last four glacial cycles (423 kyr) compared to reference simulation over last two glacial cycles (210 kyr) with identical parameters.

5.2 Ocean forcing pulse at Antarctic Cold reversal

Recent studies of coupled ice sheet and ocean dynamics (e.g. Golledge et al., 2014; Fogwill et al., 2017) suggest the idea of a positive feedback mechanism causing episodes of accelerated ice-sheet recession as result of enhanced sub-shelf melt, in particular in an ocean warming event during Antarctic Cold Reversal coincident with meltwater pulse 1A. For comparably small changes in ocean forcing (≈ 0.25 K) Golledge et al. (2014) find a three-fold mass loss from the Antarctic Ice Sheet (up to $6 \, \mathrm{mm \, yr^{-1}}$). We ran a similar sensitivity experiment with an additional ocean temperature forcing of 1 K and 2 K entering the PICO module ~~and hence~~ causing enhanced sub shelf melt.

Compared to our reference run with only 0.25 m SLE contribution during the period of two millennia (grey), we detect enhanced melt during ACR (see grey bar and dotted vertical lines in Fig. 29) with a change in volume above flotation of 0.5 m SLE (orange) and 1.6 m SLE (green) in the sensitivity experiments, which corresponds to a mean sea-level contribution rate of $0.25 \, \mathrm{mm \, yr^{-1}}$ and $0.82 \, \mathrm{mm \, yr^{-1}}$, respectively. Even though the ocean temperature forcing in the sensitivity experiments exceeds present-day level (with melt rates in the Ross and Weddell Sea above $1 \, \mathrm{m \, yr^{-1}}$), its effect on ice volume seems comparably small, as grounding lines extended to the shallow edge of the continental shelf with rather small ice shelves attached. Accordingly, PICO responds with less overturning and melt as it would for a modern configuration of the Antarctic Ice Sheet and ice shelves. Counterintuitively, the intensified ocean forcing early in the deglaciation phase has a delaying effect for the timing of the remaining deglaciation through the Holocene.
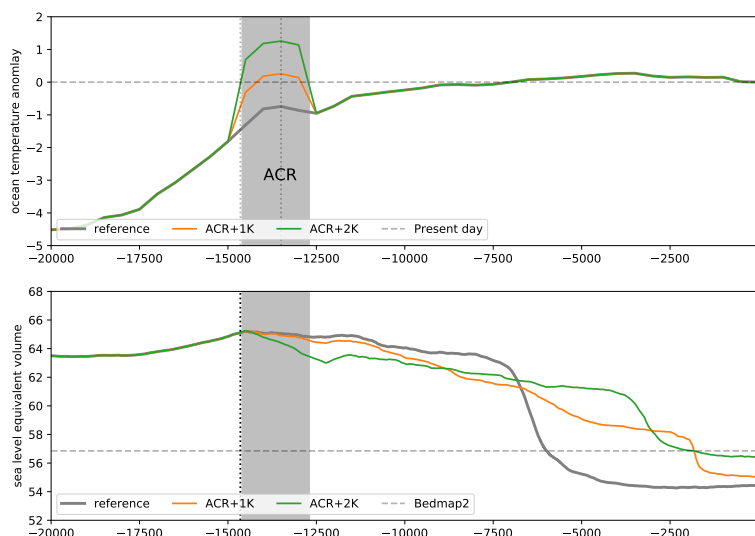
Figure 29: Simulation over two glacial cycles (only last 20 kyr shown here) with different ocean temperature forcing increased by 1 K or 2 K in the two-millenia phase (14.6-12.7 kyr BP) of Antarctic Cold Reversal after MWP1a (lower panel). The additional melt causes a doubling or even 6-fold increase in early ice volume losses, respectively, but most of the ice sheet retreat is somewhat delayed.

5.3 Conditions for earlier deglaciation

710   A timeseries of well-dated sediment data of iceberg-rafted debris (Weber et al., 2014) suggest that the main retreat of the Antarctic Ice Sheet occurred 14.6 kyr BP, as a consequence of MWP1a. Yet, in our reference simulation the main retreat occurs not before 10 kyr BP. From our sensitivity experiments we can identify relevant model parameters and boundary conditions that affect the timing of the last deglaciation. We find some tendency that no SSA enhancement ($E_{SSA} = 1$) and weaker

715   eigencalving ($K = 1 \times 10^{16}$ m s) can lead to somewhat earlier retreat (see Sect. 2). Figure 30 shows the individual effects on the ice volume history. Also for a more realistic temperature distribution (Racmo2.3p2, but without PDD, see Sect. 3.1), or for un delayed ocean temperature forcing (WDC reconstruction scaled by a factor of 0.42, see Sect. 4.3) we find earlier deglaciation. Slightly earlier retreat is simulated also for scaled sea-level forcing to mimick self-gravitational effects (Sect. 4.1),

720   as the reduced forcing passes the critical thresholds earlier. However, with only linear sampling of the parameter space we cannot draw robust conclusions for the timing, also with regard to the strong non-linearity of the system in this period (Sect. 5.1). The assumption of saturated till water in the

marine section (Sect. 3.4.3), ~~where grounding line can potentially advance to,~~ seems to be of high
relevance ~~also~~ for the timing initial grounding line retreat, with the main deglaciation initiated right
after the MWP1a. This signal also dominates the combined effect of all ~~here indicated~~ model settings
and needs to be investigated more systematically for PISM simulations (see Fig. 30).

725
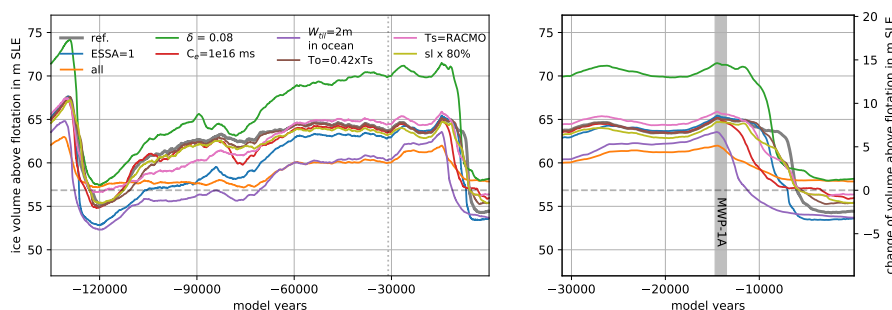
Figure 30: Individual and combined effects of model choices that lead to earlier deglaciation in
glacial cycle simulations. SSA enhancement $E_{\mathrm{SSA}} = 1$ (blue) and scaled ocean temperature forcing
(brown) cause about $2\,\mathrm{kyr}$ earlier retreat, more realistic surface temperatures (rose) and a higher
effective overburden fraction of 8% (green) cause 3–4 kyr earlier retreat, and eigencalving constant
$K = 1 \times 10^{16}\,\mathrm{m\,s}$ (red) and saturated tillwat on the ocean floor (purple) even 6 kyr earlier retreat.
Also, deglaciation with all combined effects occurs more than 6 kyr ahead of the reference (orange
and grey) and coincides with MWP1a around 14.5 kyr BP (grey vertical bar).

5.4 Grounding line sensitivity

In PISM the location of the grounding line is determined by the flotation condition (cf. $H = h_f$ in
Eq. (2)), while at the same time it affects the overall stress balance and hence the ice sheet evolution.

730 We simulate sub-grid basal friction and basal melt according to interpolated grounding line location
between grounded ice sheet and floating ice shelf (Gladstone et al., 2010). Hence, grounding-line
migration can be reasonable well represented in PISM (compared to full Stokes), even for coarse
resolution (Pattyn et al., 2013; Feldmann et al., 2014). The sensitivity of grounding line motion also
depends on applied boundary conditions. The availability of sub-glacial or sub-shelf melt water in

735 the vicinity of the grounding line may enhance ice flow or thinning, respectively. These model choice
induce some additional uncertainty, as has been indicated ~~as 'low' and 'high' scenario~~ in Golledge
et al. (2015).

Saturated till at the grounding line hampers grounding line advance and amplifies grounding line
retreat (see Fig. 31, orange and green vs. grey). A more slippery grounding line has been ~~often~~ en-

740 forced in PISM simulations before, and for it appears to have similar effect as the model improvement
described in Sect. 3.4.3. Both show much earlier deglaciation from a less extended glacial state. If

interpolation of basal melting across the grounding zone boundary is omitted (and only basal shear stress is interpolated) we also find a slower ice sheet growth and a slightly earlier deglaciation from a similar glacial state as for the reference simulation (see Fig. 31, blue vs. grey). This result may no be intuitive, but it shows that interpolation is defined symmetrically to both sides of the non-interpolated grounding line location and interpolation of basal melt can support grounding line advance. Another aspect that can potentially affect till water content and hence sliding in ice stream regions is related to the temperate ice thermal conductivity ratio, which is used to simulate a physical jump condition in the enthalpy gradient for temperate ice at the base, such that the energy at the base is balanced by the basal melting (Kleiner et al., 2015). In the reference simulation we use a very low temperate ice thermal conductivity ratio of 1×10^{-5} as suggested by Kleiner et al. (2015). However, this ratio does not seem to have much effect on the cold-temperate transition surface and hence on the ice volume history in PISM, even when varied over four orders of magnitude (default value 0.1, see red line in Fig. 31).
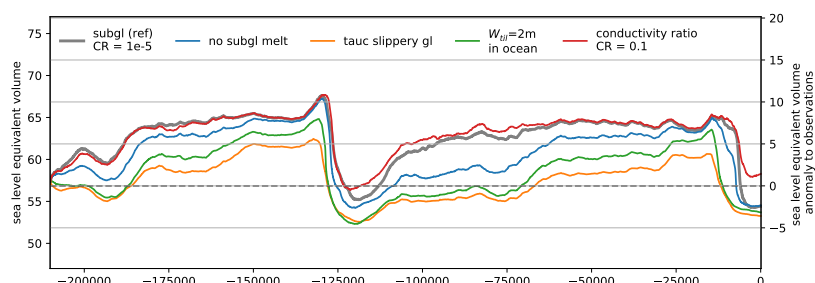
Figure 31: Sensitivity of transient ice volume above flotation to varied conditions at the grounding line. Grey curve is the reference with applied sub-grid basal shear stress and basal melt. Without interpolated basal melt (blue) PISM simulates slower grounding line advance, but faster retreat, while glacial and modern extents are comparable. Glacial ice sheet growth is even slower for enforced saturated till conditions along the marine sections of the grounding line, landward (orange) or on the ocean side of the grounding line (green). The much higher sensitivity of the ice sheet volume to climatic forcing yields a smaller glacial ice volume and much earlier deglaciation. The effect of variation of the temperate ice conductivity ratio over four orders of magnitude has only little effect, with slightly larger interglacial ice volumes for larger ratios (red).

6 Conclusions

In this study we have run PISM simulations of the Antarctic Ice Sheet over the last two glacial cycles and investigated the sensitivity of ice volume history to variations in model parameter settings,

boundary conditions and climatic forcings. Differences in ice volume above flotation are character-
ized for specific periods of the Last Interglacial, the Last Glacial Maximum (LGM) and for present
760   day. During deglaciation small perturbations can be amplified causing a strong divergence in the
ice sheet response, e.g. in the onset of deglaciation or in the maximum change rates. We quan-
tify model-intrinsic uncertainty of up to 2 m SLE for present-day climate conditions, for different
thermal initialization methods but otherwise identical model settings. Hence, simulated changes in
interglacial ice volume due to variation in parameters or boundary conditions are considered signifi-
765   cant when larger than the intrinsic uncertainty.

We find consistent results within this uncertainty range for grid resolution refinement of 16 km or
finer. Simulated ice volumes reveal only little variation for variation in SIA flow law exponent of
$n_{SIA} = 3 \pm 1$. However, in combination with variations of the SSA flow law exponent over the same
770   range, simulated ice volumes differ significantly by 2–7 m SLE. Even more significant is the effect
of the SIA enhancement factor with much thinner grounded ice for larger parameter values and a
range of simulated ice volume of up to 11 m SLE between ESIA=1–5. Increasing SSA enhancement
factors cause faster deglaciation and hence thinner modern ice sheets with up to 7 m SLE difference
for the tested parameter range of ESSA=0.3–1.0, while in contrast volumes at LGM are rather unaf-
775   fected. Calving parameters have only little effect on the simulated ice volume.

Basal friction in PISM is associated with various hydrological and microscale processes. Basal
roughness of the basal substrate expressed as till friction angle is a key parameter here. We present
an optimization algorithm for till friction angle distribution to minimize the misfit to modern ice
780   thickness. However, ice streams are reproduced less confined than with a piecewise-linear parameter-
ization dependent on bed topography. Also, the procedure cannot help to constrain basal roughness
on the continental shelf underneath the modern ice shelves. As modern ice shelf regions are covered
by grounded ice in glacial climates, a variation of minimal till friction angle of $\phi_{min} = 1.0°$–5.0°
causes 3–5 m SLE difference in ice volume above flotation for each degree, so in total up to 15 m
785   SLE difference over the tested range. Regarding the hydrological model part, variations in till wa-
ter decay rate and effective overburden pressure within a plausible range of 1–10 mm/yr and 2-8 %,
respectively, reveal additional considerable uncertainties of more than 10 m SLE each. For the ef-
fective overburden pressure, however, at least the uncertainty for modern climate conditions is much
lower. Basal sliding in PISM can account for a dependence of basal shear stress and sliding veloc-
790   ity, varying from plastic till deformation to linear sliding, expressed by the pseudo plastic exponent
PPQ. Simulated ice volumes differ for this range of PPQ=0–1 by up to 10 m SLE, both for glacial
and modern climate conditions. The basal model components are consequently the least constrained
and most sensitive parts for PISM glacial cycle simulations.

795   Within the coupled Earth model, variations in mantle viscosities over two orders of magnitude
cause slower ice sheet growth but faster deglaciation for higher values. PISM simulations yield con-
sistent present-day ice volumes for mantle viscosities of 5×10^{20} Pa s or more. The Earth model is
interactively coupled with PISM, but ~~it is~~ not globally defined and ~~has so far neglected~~ changes of
water masses around the ice sheet. We find the effect of changing sea level and bed topography for

800   the isostatic adjustment and hence on grounding line migration a relevant feedback amplifying the
ice sheet growth for glacial climates by more than 5 m SLE. In contrast, the sensitivity of ice volume
evolution to variations of the elastic part of the Earth model, expressed via the parameter for flexural
rigididy over a range of $5–100\times10^{23}$ N m, is rather low with only a few meters SLE difference. Here
we have run the latest PISM version v1.1 with a recent bug fix, revealing additional variability to

805   glacial volume history.

     In our study we present a parameterization for the ice surface temperature close to modern re-
analysis data, that accounts for changes in geometry and can be easily used in combination with the
PPD scheme. However, PDD seems to be of minor relevance in Antarctic glacial cycle simulations.

810   If annual-mean reanalysis temperatures are applied directly as modern boundary condition in com-
bination with precipitation rates from the regional climate model Racmo2.3p2, ~~both lapse corrected~~,
we find similar ice volumes at Last Glacial Maximum, but delayed growth and somewhat earlier
deglaciation. For the subsurface boundary, we find for geothermal heat flux maps ~~from different~~
~~available source comparably little difference in modeled LGM ice volume,~~ in contrast to previous

815   studies. The model spread of present-day ice volumes with up to 2 m SLE is not significant.

     In order to run glacial cycle simulations we have prescribed past external climatic ~~forcing~~ for sea-
level, ~~temperatures of the air and the ocean,~~ and for precipitation. Reconstructions of global mean
sea level use different methodologies which differ both in LGM level as well as in the rate of change

820   and timing of the last deglaciation, i.e. for the representation of meltwater pulse 1a (MWP1a). Hence,
the simulated response of the Antarctic Ice Sheet can differ by up to 5 m SLE for different ~~forcings~~.
Sea level forcing is the most dominant forcing at play together with air temperature forcing, as each
alone can trigger glaciation with ice volume growth of more than 12 m SLE above present. If no sea-
level forcing is applied, temperature and precipitation forcing balance each other and the Antarctic

825   Ice Sheet remains at modern configuration even for glacial climate conditions. Precipitation forcing
in PISM can be coupled directly to temperature forcing or can be applied as fractional anomaly to
reconstructed accumulation rates from WAIS Divide Core. For the latter case the Antarctic Ice Sheet
does not retreat from its LGM configuration until present-day due to excess accumulation trough
the Holocene. Regarding surface temperature reconstructions we compared changes with respect to

830   the choice of available cores from EPICA Dome C or WAIS Divide Core, which show only little
difference in the ice volume evolution. Even if the LGM temperatures were 40% warmer, as recent

discussions within the community suggest, we find similar glacial extents and a delayed but still effective deglaciation with less than 2.5 m SLE difference. Ocean temperature change is modeled as delayed response to changes of reconstructed air temperatures. For different response functions
835   and air temperature PISM-PICO simulates similar LGM states. However, the onset of deglaciation and hence present-day ice volume can differ by a few meters SLE. This means that, compared to the other forcings, ocean temperature forcing is of minor relevance for glacial cycle simulations. Hence, we have not varied PICO parameters in this study. Even if we enhance sub-shelf melting for 2,000 years at Antarctic Cold Reversal according to a 2 K warming in the ocean, the Antarctic Ice Sheet
840   responds with slightly earlier but slower retreat resulting in similar present-day states. We have identified model settings that allows for earlier deglacial retreat, among which the subglacial hydrology is the most dominant. But in all simulations retreat occurs after MWP1a.

From the discussed model settings and boundary conditions we select four relevant parameters
845   representative for each of the different sections. Regarding climatic forcing we identified the precipitation change rate PREC as representative parameter within the range of 2–10%/K, for the Earth model the mantle viscosity VISC within the range of $1–100×10^{20}$ Pa s, for the basal friction model the sliding exponent PPQ within the range 0.25–1.0 and for the internal ice flow dynamics the ESIA enhancement factor within the range 1–7. While ESIA and PREC are more relevant for the LGM
850   configuration of the Antarctic Ice Sheet, VISC and PPQ determine the timing and rate of deglaciation to present-day configuration. These parameter ranges define the dimensions of the large ensemble which is presented and analyzed in the companion paper (Albrecht et al., 2019).

Code and data availability

The PISM code used in this study can be obtained from https://github.com/talbrecht/pism_pik/tree/
855   pism_pik_1.0 and will be published with DOI reference. Results and plotting scripts are available upon request and will be published in www.PANGAEA.de. For now see jupyter notebook https://nbviewer.jupyter.org/url/www.pik-potsdam.de/~albrecht/notebooks/paleo_paper_final.ipynb. PISM input data are preprocessed using https://github.com/pism/pism-ais with original data citations.

Acknowledgements. Development of PISM is supported by NASA grant NNX17AG65G and NSF grants PLR-
860   1603799 and PLR-1644277. Special thanks are due to Constantine Khroulev for many years of productive PISM code development and open-source maintenance. PISM uses third-party PETSc solver libraries[5]. The authors gratefully acknowledge the European Regional Development Fund (ERDF), the German Federal Ministry of Education and Research and the Land Brandenburg for supporting this project by providing resources on the high performance computer system at the Potsdam Institute for Climate Impact Research. Computer resources

---

[5]https://www.mcs.anl.gov/petsc/

865 for this project have been also provided by the Gauss Centre for Supercomputing/Leibniz Supercomputing Cen-
tre (www.lrz.de) under Project-ID pr94ga. T.A. is supported by the Deutsche Forschungsgemeinschaft (DFG)
in the framework of the priority program "Antarctic Research with comparative investigations in Arctic ice ar-
eas" by grant LE1448/6-1 and LE1448/7-1. We thank Melchior van Wessem for providing surface forcing data
sets from RACMO2.3p2, Dick Peltier for the sea-level anomalies, Christo Buizert for the WDC temperature re-

870 constructions before publication. We are also grateful to Xylar Asay-Davis, Thomas Kleiner, Matthias Mengel,
Mark Pittard, Dave Pollard, Ronja Reese, Eric Steig and Pippa Whitehouse for constructive discussions.

References

Albrecht, T.: Movie: Reference PISM simulation of the Antarctic Ice Sheet over the past 210 kyr, Copernicus Publications, https://doi.org/10.5446/41779, 2019.

875 Albrecht, T. and Levermann, A.: Spontaneous ice-front retreat caused by disintegration of adjacent ice shelf in Antarctica, Earth and Planetary Science Letters, 393, 26–30, 2014.

Albrecht, T., Winkelmann, R., and Levermann, A.: Glacial cycles simulation of the Antarctic Ice Sheet with PISM - Part 2: Parameter ensemble analysis, The Cryosphere Discussions, 2019, doi:10.5194/tc-2019-70, https://www.the-cryosphere-discuss.net/tc-2019-70/, 2019.

880 An, M., Wiens, D. A., Zhao, Y., Feng, M., Nyblade, A., Kanao, M., Li, Y., Maggi, A., and Lévêque, J.-J.: Temperature, lithosphere-asthenosphere boundary, and heat flux beneath the Antarctic Plate inferred from seismic velocities, Journal of Geophysical Research: Solid Earth, 120, 8720–8742, 2015.

Aschwanden, A. and Blatter, H.: Mathematical modeling and numerical simulation of polythermal glaciers, Journal of Geophysical Research: Earth Surface, 114, 2009.

885 Aschwanden, A., Bueler, E., Khroulev, C., and Blatter, H.: An enthalpy formulation for glaciers and ice sheets, Journal of Glaciology, 58, 441–457, doi:10.3189/2012JoG11J088, 2012.

Aschwanden, A., Fahnestock, M. A., and Truffer, M.: Complex Greenland outlet glacier flow captured, Nature communications, 7, 10 524, 2016.

Bakker, P., Clark, P. U., Golledge, N. R., Schmittner, A., and Weber, M. E.: Centennial-scale Holocene climate
890 variations amplified by Antarctic Ice Sheet discharge, Nature, 541, 72, 2017.

Barletta, V. R., Bevis, M., Smith, B. E., Wilson, T., Brown, A., Bordoni, A., Willis, M., Khan, S. A., Rovira-Navarro, M., Dalziel, I., et al.: Observed rapid bedrock uplift in Amundsen Sea Embayment promotes ice-sheet stability, Science, 360, 1335–1339, 2018.

Bindschadler, R. A., Nowicki, S., Abe-Ouchi, A., Aschwanden, A., Choi, H., Fastook, J., Granzow, G., Greve,
895 R., Gutowski, G., Herzfeld, U., et al.: Ice-sheet model sensitivities to environmental forcing and their use in projecting future sea level (the SeaRISE project), Journal of Glaciology, 59, 195–224, 2013.

Bintanja, R. and Van de Wal, R.: North American ice-sheet dynamics and the onset of 100,000-year glacial cycles, Nature, 454, 869–872, 2008.

Bons, P. D., Kleiner, T., Llorens, M.-G., Prior, D. J., Sachau, T., Weikusat, I., and Jansen, D.: Greenland Ice
900 Sheet: Higher nonlinearity of ice flow significantly reduces estimated basal motion, Geophysical Research Letters, 45, 6542–6548, 2018.

Briggs, R., Pollard, D., and Tarasov, L.: A glacial systems model configured for large ensemble analysis of Antarctic deglaciation, The Cryosphere, 7, 1949–1970, 2013.

Briggs, R. D., Pollard, D., and Tarasov, L.: A data-constrained large ensemble analysis of Antarctic evolution
905 since the Eemian, Quaternary Science Reviews, 103, 91–115, doi:10.1016/j.quascirev.2014.09.003, 2014.

Brondex, J., Gagliardini, O., Gillet-Chaulet, F., and Durand, G.: Sensitivity of grounding line dynamics to the choice of the friction law, Journal of Glaciology, 63, 854–866, 2017.

Bueler, E. and Brown, J.: Shallow shelf approximation as a "sliding law" in a thermomechanically coupled ice sheet model, Journal of Geophysical Research, 114, doi:10.1029/2008JF001179, 2009.

910 Bueler, E. and van Pelt, W.: Mass-conserving subglacial hydrology in the Parallel Ice Sheet Model version 0.6, Geoscientific Model Development, 8, 1613, 2015.

Bueler, E., Lingle, C. S., and Brown, J.: Fast computation of a viscoelastic deformable Earth model for ice-sheet
simulations, Annals of Glaciology, 46, 97–105, 2007.

Buizert, C., Cuffey, K., Severinghaus, J., Baggenstos, D., Fudge, T., Steig, E., Markle, B., Winstrup, M., Rhodes,
915   R., Brook, E., et al.: The WAIS Divide deep ice core WD2014 chronology–Part 1: Methane synchronization
(68–31 ka BP) and the gas age–ice age difference, Climate of the Past, 11, 153–173, 2015.

Chen, B., Haeger, C., Kaban, M. K., and Petrunin, A. G.: Variations of the effective elastic thickness reveal
tectonic fragmentation of the Antarctic lithosphere, Tectonophysics, 746, 412–424, 2018.

Cuffey, K. M. and Paterson, W. S. B.: The physics of glaciers, Academic Press, 2010.

920   Cuffey, K. M., Clow, G. D., Steig, E. J., Buizert, C., Fudge, T., Koutnik, M., Waddington, E. D., Alley, R. B., and
Severinghaus, J. P.: Deglacial temperature history of West Antarctica, Proceedings of the National Academy
of Sciences, 113, 14 249–14 254, http://www.usap-dc.org/view/dataset/600377, 2016.

de Fleurian, B., Werder, M. A., Beyer, S., Brinkerhoff, D. J., Delaney, I., Dow, C. F., Downs, J., Gagliardini,
O., Hoffman, M. J., Hooke, R. L., et al.: SHMIP The subglacial hydrology model intercomparison Project,
925   Journal of Glaciology, 64, 897–916, 2018.

Depoorter, M. A., Bamber, J., Griggs, J., Lenaerts, J., Ligtenberg, S. R., Van den Broeke, M., and Moholdt, G.:
Calving fluxes and basal melt rates of Antarctic ice shelves, Nature, 502, 89, 2013.

Doake, C., Corr, H., Rott, H., Skvarca, P., and Young, N.: Breakup and conditions for stability of the northern
Larsen Ice Shelf, Antarctica, Nature, 391, 778, 1998.

930   Edwards, T. L., Brandon, M. A., Durand, G., Edwards, N. R., Golledge, N. R., Holden, P. B., Nias, I. J., Payne,
A. J., Ritz, C., and Wernecke, A.: Revisiting Antarctic ice loss due to marine ice-cliff instability, Nature, 566,
58, 2019.

Falcini, F. A., Rippin, D. M., Krabbendam, M., and Selby, K. A.: Quantifying bed roughness beneath contem-
porary and palaeo-ice streams, Journal of Glaciology, 64, 822–834, 2018.

935   Feldmann, J. and Levermann, A.: Collapse of the West Antarctic Ice Sheet after local destabiliza-
tion of the Amundsen Basin, Proceedings of the National Academy of Sciences, p. 201512482,
doi:10.1073/pnas.1512482112, http://www.pnas.org/lookup/doi/10.1073/pnas.1512482112, 2015.

Feldmann, J. and Levermann, A.: From cyclic ice streaming to Heinrich-like events: the grow-and-surge insta-
bility in the Parallel Ice Sheet Model, The Cryosphere, 11, 1913–1932, 2017.

940   Feldmann, J., Albrecht, T., Khroulev, C., Pattyn, F., and Levermann, A.: Resolution-dependent performance of
grounding line motion in a shallow model compared with a full-Stokes model according to the MISMIP3d
intercomparison, Journal of Glaciology, 60, 353–360, doi:10.3189/2014JoG13J093, 2014.

Fogwill, C., Turney, C., Golledge, N., Etheridge, D., Rubino, M., Thornton, D., Baker, A., Woodward, J.,
Winter, K., Van Ommen, T., et al.: Antarctic ice sheet discharge driven by atmosphere-ocean feedbacks at
945   the Last Glacial Termination, Scientific reports, 7, 39 979, 2017.

Fowler, A.: A theoretical treatment of the sliding of glaciers in the absense of cavitation, Phil. Trans. R. Soc.
Lond. A, 298, 637–681, 1981.

Fox Maule, C., Purucker, M. E., Olsen, N., and Mosegaard, K.: Heat Flux Anomalies in Antarctica Revealed
by Satellite Magnetic Data, Science, 309, 464–467, doi:10.1126/science.1106888, 2005.

950   Fretwell, P., Pritchard, H. D., Vaughan, D. G., Bamber, J. L., Barrand, N. E., Bell, R., Bianchi, C., Bingham,
R. G., Blankenship, D. D., Casassa, G., Catania, G., Callens, D., Conway, H., Cook, A. J., Corr, H. F. J.,

Damaske, D., Damm, V., Ferraccioli, F., Forsberg, R., Fujita, S., Gim, Y., Gogineni, P., Griggs, J. A., Hind-
marsh, R. C. A., Holmlund, P., Holt, J. W., Jacobel, R. W., Jenkins, A., Jokat, W., Jordan, T., King, E. C.,
Kohler, J., Krabill, W., Riger-Kusk, M., Langley, K. A., Leitchenkov, G., Leuschen, C., Luyendyk, B. P.,
955 Matsuoka, K., Mouginot, J., Nitsche, F. O., Nogi, Y., Nost, O. A., Popov, S. V., Rignot, E., Rippin, D. M.,
Rivera, A., Roberts, J., Ross, N., Siegert, M. J., Smith, A. M., Steinhage, D., Studinger, M., Sun, B., Tinto,
B. K., Welch, B. C., Wilson, D., Young, D. A., Xiangbin, C., and Zirizzotti, A.: Bedmap2: improved ice
bed, surface and thickness datasets for Antarctica, The Cryosphere, 7, 375–393, doi:10.5194/tc-7-375-2013,
https://secure.antarctica.ac.uk/data/bedmap2/, 2013.

960 Frieler, K., Clark, P. U., He, F., Buizert, C., Reese, R., Ligtenberg, S. R. M., van den Broeke, M. R., Winkelmann,
R., and Levermann, A.: Consistent evidence of increasing Antarctic accumulation with warming, Nature
Climate Change, 5, 348–352, doi:10.1038/nclimate2574, 2015.

Fudge, T., Markle, B. R., Cuffey, K. M., Buizert, C., Taylor, K. C., Steig, E. J., Waddington, E. D., Conway, H.,
and Koutnik, M.: Variable relationship between accumulation and temperature in West Antarctica for the past
965 31,000 years, Geophysical Research Letters, 43, 3795–3803, http://www.usap-dc.org/view/dataset/601004,
2016.

Fürst, J. J., Durand, G., Gillet-Chaulet, F., Tavard, L., Rankl, M., Braun, M., and Gagliardini, O.: The safety
band of Antarctic ice shelves, Nature Climate Change, 6, 479, 2016.

Gasson, E., DeConto, R., and Pollard, D.: Antarctic bedrock topography uncertainty and ice sheet stability,
970 Geophysical Research Letters, 42, 5372–5377, 2015.

Gillet-Chaulet, F., Durand, G., Gagliardini, O., Mosbeux, C., Mouginot, J., Rémy, F., and Ritz, C.: Assimilation
of surface velocities acquired between 1996 and 2010 to constrain the form of the basal friction law under
Pine Island Glacier, Geophysical Research Letters, 43, 2016.

Gladstone, R., Schäfer, M., Zwinger, T., Gong, Y., Strozz, T., Moore, J., Mottram, R., and Boberg, F.: Im-
975 portance of basal processes in simulations of a surging Svalbard outlet glacier., Cryosphere Discussions, 7,
2013.

Gladstone, R. M., Payne, A. J., and Cornford, S. L.: Parameterising the grounding line in flow-line ice sheet
models, The Cryosphere, 4, 605–619, doi:10.5194/tc-4-605-2010, 2010.

Gladstone, R. M., Payne, A. J., and Cornford, S. L.: Resolution requirements for grounding-line modelling:
980 sensitivity to basal drag and ice-shelf buttressing, Annals of glaciology, 53, 97–105, 2012.

Gladstone, R. M., Warner, R. C., Galton-Fenzi, B. K., Gagliardini, O., Zwinger, T., and Greve, R.: Marine
ice sheet model performance depends on basal sliding physics and sub-shelf melting, The Cryosphere, 11,
319–329, 2017.

Goldsby, D. and Kohlstedt, D.: Superplastic deformation of ice: Experimental observations, Journal of Geo-
985 physical Research: Solid Earth, 106, 11 017–11 030, 2001.

Golledge, N. R., Menviel, L., Carter, L., Fogwill, C. J., England, M. H., Cortese, G., and Levy, R. H.: Antarctic
contribution to meltwater pulse 1A from reduced Southern Ocean overturning, Nature Communications, 5,
doi:10.1038/ncomms6107, 00000, 2014.

Golledge, N. R., Kowalewski, D. E., Naish, T. R., Levy, R. H., Fogwill, C. J., and Gasson, E. G.: The multi-
990 millennial Antarctic commitment to future sea-level rise, Nature, 526, 421–425, 2015.

Golledge, N. R., Keller, E. D., Gomez, N., Naughten, K. A., Bernales, J., Trusel, L. D., and Edwards, T. L.:
Global environmental consequences of twenty-first-century ice-sheet melt, Nature, 566, 65, 2019.

Gomez, N., Pollard, D., and Mitrovica, J. X.: A 3-D coupled ice sheet–sea level model applied to Antarctica
through the last 40 ky, Earth and Planetary Science Letters, 384, 88–99, 2013.

995 Halberstadt, A. R. W., Simkins, L. M., Anderson, J. B., Prothro, L. O., and Bart, P. J.: Characteristics of the
deforming bed: till properties on the deglaciated Antarctic continental shelf, Journal of Glaciology, 64, 1014–
1027, 2018.

Hay, C. C., Lau, H. C., Gomez, N., Austermann, J., Powell, E., Mitrovica, J. X., Latychev, K., and Wiens,
D. A.: Sea level fingerprints in a region of complex Earth structure: The case of WAIS, Journal of Climate,
1000 30, 1881–1892, 2017.

Huybrechts, P. and de Wolde, J.: The dynamic response of the Greenland and Antarctic ice sheets to multiple-
century climatic warming, Journal of Climate, 12, 2169–2188, 1999.

Imbrie, J. D. and McIntyre, A.: SPECMAP time scale developed by Imbrie et al., 1984 based on normalized
planktonic records (normalized O-18 vs time, specmap.017), 10.1594/PANGAEA.4417068, 2006.

1005 Jouzel, J., Masson-Delmotte, V., Cattani, O., Dreyfus, G., Falourd, S., Hoffmann, G., Minster, B., Nouet, J.,
Barnola, J. M., Chappellaz, J., Fischer, H., Gallet, J. C., Johnsen, S., Leuenberger, M., Loulergue, L., Luethi,
D., Oerter, H., Parrenin, F., Raisbeck, G., Raynaud, D., Schilt, A., Schwander, J., Selmo, E., Souchez, R.,
Spahni, R., Stauffer, B., Steffensen, J. P., Stenni, B., Stocker, T. F., Tison, J. L., Werner, M., and Wolff,
E. W.: Orbital and Millennial Antarctic Climate Variability over the Past 800,000 Years, Science, 317, 793–
1010 796, doi:10.1126/science.1141038, 2007.

Kingslake, J., Scherer, R., Albrecht, T., Coenen, J., Powell, R., Reese, R., Stansell, N., Tulaczyk, S., Wearing,
M., and Whitehouse, P.: Extensive retreat and re-advance of the West Antarctic ice sheet during the Holocene,
Nature, 558, 430, 2018.

Kleiner, T., Rückamp, M., Bondzio, J. H., and Humbert, A.: Enthalpy benchmark experiments for numerical
1015 ice sheet models, The Cryosphere, 9, 217–228, doi:10.5194/tc-9-217-2015, https://www.the-cryosphere.net/
9/217/2015/, 2015.

Konrad, H., Sasgen, I., Pollard, D., and Klemann, V.: Potential of the solid-Earth response for limiting long-term
West Antarctic Ice Sheet retreat in a warming climate, Earth and Planetary Science Letters, 432, 254–264,
2015.

1020 Lambeck, K., Rouby, H., Purcell, A., Sun, Y., and Sambridge, M.: Sea level and global ice volumes from the
Last Glacial Maximum to the Holocene, Proceedings of the National Academy of Sciences, 111, 15 296–
15 303, doi:10.1073/pnas.1411762111, 2014.

Larour, E., Seroussi, H., Morlighem, M., and Rignot, E.: Continental scale, high order, high spatial resolu-
tion, ice sheet modeling using the Ice Sheet System Model (ISSM), Journal of Geophysical Research: Earth
1025 Surface, 117, 2012.

Levermann, A., Albrecht, T., Winkelmann, R., Martin, M., Haseloff, M., and Joughin, I.: Kinematic first-order
calving law implies potential for abrupt ice-shelf retreat, The Cryosphere, 6, 273–286, 2012.

Li, C., Storch, J.-S. v., and Marotzke, J.: Deep-ocean heat uptake and equilibrium climate response, Climate
Dynamics, 40, 1071–1086, doi:10.1007/s00382-012-1350-z, 2012.

1030 Lisiecki, L. E.: Links between eccentricity forcing and the 100,000-year glacial cycle, Nature geoscience, 3, 349, 2010.

Lisiecki, L. E. and Raymo, M. E.: A Pliocene-Pleistocene stack of 57 globally distributed benthic $\delta18$O records, Paleoceanography, 20, 2005.

Liu, J., Milne, G. A., Kopp, R. E., Clark, P. U., and Shennan, I.: Sea-level constraints on the amplitude and
1035 source distribution of Meltwater Pulse 1A, Nature Geoscience, 9, 130–134, doi:10.1038/ngeo2616, 2016.

Lliboutry, L. and Duval, P.: Various isotropic and anisotropic ices found in glaciers and polar ice caps and their corresponding rheologies: Ann Geophys V3, N2, March–April 1985, P207–224, in: International Journal of Rock Mechanics and Mining Sciences & Geomechanics Abstracts, vol. 22, p. 198, Pergamon, 1985.

Ma, Y., Gagliardini, O., Ritz, C., Gillet-Chaulet, F., Durand, G., and Montagnat, M.: Enhancement factors for
1040 grounded ice and ice shelves inferred from an anisotropic ice-flow model, Journal of Glaciology, 56, 805–812, http://www.ingentaconnect.com/content/igsoc/jog/2010/00000056/00000199/art00006, 2010.

Maris, M., De Boer, B., Ligtenberg, S., Crucifix, M., Van De Berg, W., and Oerlemans, J.: Modelling the evolution of the Antarctic ice sheet since the last interglacial, The Cryosphere, 8, 1347–1360, 2014.

Martin, M. A., Winkelmann, R., Haseloff, M., Albrecht, T., Bueler, E., Khroulev, C., and Levermann, A.: The
1045 Potsdam Parallel Ice Sheet Model (PISM-PIK) – Part 2: Dynamic equilibrium simulation of the Antarctic ice sheet, The Cryosphere, 5, 727–740, doi:10.5194/tc-5-727-2011, http://www.the-cryosphere.net/5/727/2011/, 2011.

Martos, Y. M., Catalán, M., Jordan, T. A., Golynsky, A., Golynsky, D., Eagles, G., and Vaughan, D. G.: Heat flux distribution of Antarctica unveiled, Geophysical Research Letters, 44, 2017.

1050 Mengel, M. and Levermann, A.: Ice plug prevents irreversible discharge from East Antarctica, Nature Climate Change, 4, 451–455, doi:10.1038/nclimate2226, http://www.nature.com/doifinder/10.1038/nclimate2226, 2014.

Mengel, M., Feldmann, J., and Levermann, A.: Linear sea-level response to abrupt ocean warming of major West Antarctic ice basin, Nature Climate Change, 6, 71–74, 2016.

1055 Morlighem, M., Williams, C. N., Rignot, E., An, L., Arndt, J. E., Bamber, J. L., Catania, G., Chauché, N., Dowdeswell, J. A., Dorschel, B., et al.: BedMachine v3: Complete bed topography and ocean bathymetry mapping of Greenland from multibeam echo sounding combined with mass conservation, Geophysical research letters, 44, 2017.

Nowicki, S. M., Payne, A., Larour, E., Seroussi, H., Goelzer, H., Lipscomb, W., Gregory, J., Abe-Ouchi, A.,
1060 and Shepherd, A.: Ice Sheet Model Intercomparison Project (ISMIP6) contribution to CMIP6, Geoscientific Model Development, 9, 4521, 2016.

Pattyn, F.: The paradigm shift in Antarctic ice sheet modelling, Nature communications, 9, 2728, 2018.

Pattyn, F., Perichon, L., Durand, G., Favier, L., Gagliardini, O., Hindmarsh, R. C., Zwinger, T., Albrecht, T., Cornford, S., Docquier, D., et al.: Grounding-line migration in plan-view marine ice-sheet models: results of
1065 the ice2sea MISMIP3d intercomparison, Journal of Glaciology, 59, 410–422, 2013.

Pittard, M., Galton-Fenzi, B., Roberts, J., and Watson, C.: Organization of ice flow by localized regions of elevated geothermal heat flux, Geophysical Research Letters, 43, 3342–3350, 2016.

Pollard, D. and DeConto, R.: Description of a hybrid ice sheet-shelf model, and application to Antarctica, Geoscientific Model Development, 5, 1273, 2012a.

1070 Pollard, D. and DeConto, R. M.: Modelling West Antarctic ice sheet growth and collapse through the past five
      million years, Nature, 458, 329–332, 2009.

Pollard, D. and DeConto, R. M.: A simple inverse method for the distribution of basal sliding coefficients
      under ice sheets, applied to Antarctica, The Cryosphere, 6, 953–971, doi:10.5194/tc-6-953-2012, http://www.
      the-cryosphere.net/6/953/2012/, 2012b.

1075 Pollard, D., Chang, W., Haran, M., Applegate, P., and DeConto, R.: Large ensemble modeling of the last
      deglacial retreat of the West Antarctic Ice Sheet: comparison of simple and advanced statistical techniques,
      Geosci. Model Dev., 9, 1697–1723, doi:10.5194/gmd-9-1697-2016, 2016.

Pollard, D., Gomez, N., and Deconto, R. M.: Variations of the Antarctic Ice Sheet in a Coupled Ice Sheet-
      Earth-Sea Level Model: Sensitivity to Viscoelastic Earth Properties, Journal of Geophysical Research: Earth
1080 Surface, 122, 2124–2138, 2017.

Purucker, M.: Geothermal heat flux data set based on low resolution observations collected by the CHAMP
      satellite between 2000 and 2010, and produced from the MF-6 model following the technique described in
      Fox Maule et al.(2005), 2013.

Quiquet, A., Punge, H. J., Ritz, C., Fettweis, X., Gallée, H., Kageyama, M., Krinner, G., Salas y Mélia, D.,
1085 and Sjolte, J.: Sensitivity of a Greenland ice sheet model to atmospheric forcing fields, The Cryosphere, 6,
      999–1018, doi:10.5194/tc-6-999-2012, https://www.the-cryosphere.net/6/999/2012/, 2012.

Reese, R., Albrecht, T., Mengel, M., Asay-Davis, X., and Winkelmann, R.: Antarctic sub-shelf melt rates via
      PICO, The Cryosphere, 12, 1969, 2018.

Ritz, C., Fabre, A., and Letréguilly, A.: Sensitivity of a Greenland ice sheet model to ice flow and ablation
1090 parameters: consequences for the evolution through the last climatic cycle, Climate Dynamics, 13, 11–23,
      doi:10.1007/s003820050149, https://doi.org/10.1007/s003820050149, 1996.

Schmidtko, S., Heywood, K. J., Thompson, A. F., and Aoki, S.: Multidecadal warming of Antarctic waters,
      Science, 346, 1227–1231, 2014.

Schoof, C.: The effect of cavitation on glacier sliding, in: Proceedings of the Royal Society of London A:
1095 Mathematical, Physical and Engineering Sciences, vol. 461, pp. 609–627, The Royal Society, 2005.

Schoof, C.: Variational methods for glacier flow over plastic till, Journal of Fluid Mechanics, 555, 299–320,
      2006.

Schoof, C.: Marine ice-sheet dynamics. Part 1. The case of rapid sliding, Journal of Fluid Mechanics, 573, 27,
      doi:10.1017/S0022112006003570, 2007a.

1100 Schoof, C.: Ice sheet grounding line dynamics: Steady states, stability, and hysteresis, Journal of Geophysical
      Research, 112, doi:10.1029/2006JF000664, http://doi.wiley.com/10.1029/2006JF000664, 2007b.

Schoof, C.: Coulomb friction and other sliding laws in a higher-order glacier flow model, Mathematical Models
      and Methods in Applied Sciences, 20, 157–189, 2010.

Shapiro, N. M. and Ritzwoller, M. H.: Inferring surface heat flux distributions guided by a global seismic model:
1105 particular application to Antarctica, Earth and Planetary Science Letters, 223, 213–224, 2004.

Siegert, M. J., Jamieson, S. S., and White, D.: Exploration of subsurface Antarctica: uncovering past changes
      and modern processes, Geological Society, London, Special Publications, 461, 1–6, 2018.

Simmons, A.: ERA-Interim: New ECMWF reanalysis products from 1989 onwards, ECMWF newsletter, 110,
      25–36, 2006.

1110   Spratt, R. M. and Lisiecki, L. E.: A Late Pleistocene sea level stack, Climate of the Past, 12, 1079, 2016.

Stuhne, G. and Peltier, W.: Assimilating the ICE-6G_C Reconstruction of the Latest Quaternary Ice Age Cycle Into Numerical Simulations of the Laurentide and Fennoscandian Ice Sheets, Journal of Geophysical Research: Earth Surface, 122, 2324–2347, 2017.

Stuhne, G. R. and Peltier, W. R.: Reconciling the ICE-6G_C reconstruction of glacial chronology with ice sheet
1115   dynamics: The cases of Greenland and Antarctica, Journal of Geophysical Research: Earth Surface, 120, 2015JF003 580, doi:10.1002/2015JF003580, 2015.

Sun, S., Cornford, S., Liu, Y., and Moore, J. C.: Dynamic response of Antarctic ice shelves to bedrock uncertainty, The Cryosphere, 8, 1561–1576, 2014.

Sutter, J., Fischer, H., Grosfeld, K., Karlsson, N. B., Kleiner, T., Van Liefferinge, B., and Eisen, O.:
1120   Modelling the Antarctic Ice Sheet across the Mid Pleistocene Transition – Implications for Oldest Ice, The Cryosphere Discussions, 2019, 1–24, doi:10.5194/tc-2019-24, https://www.the-cryosphere-discuss.net/tc-2019-24/, 2019.

The PISM authors: PISM, a Parallel Ice Sheet Model: User's Manual, http://pism-docs.org/sphinx/, based on revision stable v.1.0 edn., 2017.

1125   Van de Berg, W., Van den Broeke, M., Reijmer, C., and Van Meijgaard, E.: Characteristics of the Antarctic surface mass balance, 1958–2002, using a regional atmospheric climate model, Annals of Glaciology, 41, 97–104, 2005.

Weber, M. E., Clark, P. U., Kuhn, G., Timmermann, A., Sprenk, D., Gladstone, R., Zhang, X., Lohmann, G., Menviel, L., Chikamoto, M. O., Friedrich, T., and Ohlwein, C.: Millennial-scale variability in Antarctic ice-
1130   sheet discharge during the last deglaciation, Nature, 510, 134–138, doi:10.1038/nature13397, 00002, 2014.

Werner, M., Jouzel, J., Masson-Delmotte, V., and Lohmann, G.: Reconciling glacial Antarctic water stable isotopes with ice sheet topography and the isotopic paleothermometer, Nature communications, 9, 3537, 2018.

Wessem, J. M. v., Berg, W. J. v. d., Noël, B. P., Meijgaard, E. v., Amory, C., Birnbaum, G., Jakobs, C. L.,
1135   Krüger, K., Lenaerts, J., Lhermitte, S., et al.: Modelling the climate and surface mass balance of polar ice sheets using RACMO2–Part 2: Antarctica (1979–2016), The Cryosphere, 12, 1479–1498, 2018.

Whitehouse, P. L.: Glacial isostatic adjustment modelling: historical perspectives, recent advances, and future directions, Earth Surface Dynamics, 6, 401–429, 2018.

Whitehouse, P. L., Bentley, M. J., Milne, G. A., King, M. A., and Thomas, I. D.: A new glacial isostatic ad-
1140   justment model for Antarctica: calibrated and tested using observations of relative sea-level change and present-day uplift rates, Geophysical Journal International, 190, 1464–1482, 2012.

Whitehouse, P. L., Gomez, N., King, M. A., and Wiens, D. A.: Solid Earth change and the evolution of the Antarctic Ice Sheet, Nature communications, 10, 503, 2019.

Winkelmann, R. and Levermann, A.: Linear response functions to project contributions to future sea level,
1145   Climate dynamics, 40, 2579–2588, 2013.

Winkelmann, R., Martin, M. A., Haseloff, M., Albrecht, T., Bueler, E., Khroulev, C., and Levermann, A.: The Potsdam Parallel Ice Sheet Model (PISM-PIK) – Part 1: Model description, The Cryosphere, 5, 715–726, doi:10.5194/tc-5-715-2011, 2011.

Winkelmann, R., Levermann, A., Ridgwell, A., and Caldeira, K.: Combustion of available fossil fuel resources
sufficient to eliminate the Antarctic Ice Sheet, Science advances, 1, e1500589, 2015.

Yu, H., Rignot, E., Morlighem, M., and Seroussi, H.: Iceberg calving of Thwaites Glacier, West Antarctica: full-
Stokes modeling combined with linear elastic fracture mechanics, The Cryosphere, 11, 1283–1296, 2017.

1150